Neoantigen-reactive CD8+ T cells affect clinical outcome of adoptive transfer with tumor-infiltrating lymphocytes in melanoma

Nikolaj Pagh Kristensen, … , Inge Marie Svane, Sine Reker Hadrup

Clinical Research and Public Health   In-Press Preview   Immunology

BACKGROUND. Neoantigen-driven recognition and T cell-mediated killing contribute to tumor clearance following adoptive cell therapy (ACT) with Tumor-Infiltrating Lymphocytes (TILs). Yet, how diversity, frequency, and persistence of expanded neoepitope-specific CD8+ T cells derived from TIL infusion products affect patient outcome is not fully determined.

METHODS. Using barcoded pMHC multimers, we provide a comprehensive mapping of CD8+ T cells recognizing neoepitopes in TIL infusion products and blood samples from 26 metastatic mela-noma patients who received ACT.

RESULTS. We identified 106 neoepitopes within TIL infusion products corresponding to 1.8% of all predicted neoepitopes. We observed neoepitope-specific recognition to be virtually devoid in TIL infusion products given to patients with progressive disease outcome. Moreover, we found that the frequency of neoepitope-specific CD8+ T cells in TIL infusion products correlated with in-creased survival, and that detection of engrafted CD8+ T cells in post-treatment (i.e. originating from the TIL infusion product) were unique to responders of TIL-ACT. Finally, we found that a transcriptional signature for lymphocyte activity within the tumor microenvironment was associated with a higher frequency of neoepitope-specific CD8+ T cells in the infusion product.

CONCLUSIONS. These data support previous case studies of neoepitope-specific CD8+ T cells in melanoma, and indicate that successful TIL-ACT is associated with an expansion of neoepitope-specific CD8+ T cells.

Find the latest version:

Neoantigen-reactive CD8+ T cells affect clinical outcome of adoptive transfer with tumor-infiltrating lymphocytes in melanoma

Authors: Nikolaj Pagh Kristensen[1][†], Christina Heeke[1][†], Siri A. Tvingsholm[1][†], Annie Borch[1], Arianna Draghi[2], Michael D. Crowther[2], Ibel Carri[3], Kamilla K. Munk [1], Jeppe Sejerø Holm[1], Anne-Mette Bjerregaard[1], Amalie Kai Bentzen[1], Andrea M. Marquard[1], Zoltan Szallasi[4], Nicholas McGranahan[5], Rikke Andersen[2], Morten Nielsen[3, 6], Göran B. Jönsson[7], Marco Donia[2], Inge Marie Svane[2], Sine Reker Hadrup[1*]

Affiliations

[1] Section for Experimental and Translational Immunology, Department of Health Technology, Technical University of Denmark (DTU); Kgs. Lyngby, Denmark.

[2] National Center for Cancer Immune Therapy (CCIT-DK), Department of Oncology, Copenhagen University Hospital, Herlev, Denmark.

[3] Instituto de Investigaciones Biotecnológicas, Universidad Nacional de San Martín; Buenos Aires, Argentina.

[4] Danish Cancer Society Research Center; Copenhagen, Denmark.

[5] Cancer Genome Evolution Research Group, University College London Cancer Institute, London, UK.

[6] Section for Bioinformatics, Department of Health Technology, Technical University of Denmark (DTU), Kgs. Lyngby, Denmark.

[7] Division of Oncology and Pathology, Department of Clinical Sciences Lund, Faculty of Medicine, Lund University, Sweden.

†these authors share co-first authorship. *Corresponding author. Email: sirha@dtu.dk. Address: Kemitorvet bld. 204, 2800 Kgs. Lyngby. Phone: +45 27 12 52 21.

Present Affiliations

The following authors have since the completion of the work gained new affiliations: CH (CBio A/S, Copenhagen, Denmark), JSH (PokeAcell, Copenhagen, Denmark), AMB (Novo Nordisk A/S, Måløv, Denmark), and AMM (Clinical Microbiomics, Copenhagen, Denmark).

Conflict of interest

SRH is the cofounder of Immumap, Tetramer-shop and PokeAcell and is the co-inventor of the patents WO2015185067 and WO2015188839 for the barcoded MHC technology which is licenced to Immudex. The data presented in this study is not directly involved in these activities. MD has received honoraria for lectures from Novartis and Roche.

Abstract

BACKGROUND. Neoantigen-driven recognition and T cell-mediated killing contribute to tumor clearance following adoptive cell therapy (ACT) with Tumor-Infiltrating Lymphocytes (TILs). Yet, how diversity, frequency, and persistence of expanded neoepitope-specific CD8+ T cells derived from TIL infusion products affect patient outcome is not fully determined.

METHODS. Using barcoded pMHC multimers, we provide a comprehensive mapping of CD8+ T cells recognizing neoepitopes in TIL infusion products and blood samples from 26 metastatic melanoma patients who received ACT.

RESULTS. We identified 106 neoepitopes within TIL infusion products corresponding to 1.8% of all predicted neoepitopes. We observed neoepitope-specific recognition to be virtually devoid in TIL infusion products given to patients with progressive disease outcome. Moreover, we found that the frequency of neoepitope-specific CD8+ T cells in TIL infusion products correlated with increased survival, and that detection of engrafted CD8+ T cells in post-treatment (i.e. originating from the TIL infusion product) were unique to responders of TIL-ACT. Finally, we found that a transcriptional signature for lymphocyte activity within the tumor microenvironment was associated with a higher frequency of neoepitope-specific CD8+ T cells in the infusion product.

CONCLUSIONS. These data support previous case studies of neoepitope-specific CD8+ T cells in melanoma, and indicate that successful TIL-ACT is associated with an expansion of neoepitope-specific CD8+ T cells.

1 Introduction

Adoptive cell transfer with expanded tumor-infiltrating lymphocytes (TIL-ACT) can mediate durable tumor regression in patients with metastatic melanoma (1, 2). Furthermore, TIL-ACT has a high objective response rate even after the failure of checkpoint inhibitor therapy (1–4). TIL-ACT therefore represents an attractive treatment option for metastatic melanoma patients with high unmet medical needs. Current predictors of tumor regression and long-term survival after ACT include tumor-mutational burden (TMB) and neoantigen load (5), which have recently emerged as independent predictors of outcome across multiple immunotherapies (6, 7). Moreover, transcriptomic evidence implicates antigen-presentation within the tumor microenvironment before TIL-ACT (5) as an important additional factor, suggesting that antigen-presentation and immune-recognition of mutation-derived neoantigens contribute to therapeutic benefit in TIL-ACT. While immune-recognition and tumor-cell killing is generally associated with a positive outcome (8, 9), evaluation of T cell recognition to mutation-derived neoantigens within TIL infusion (Inf) products and peripheral blood after infusion have only been reported in case studies of complete responders (10–15). We aimed to systematically assess T cell recognition towards neoantigens in TIL-ACT and their influence on therapeutic outcome. Recent advances in T cell technologies have led to the possibility of comprehensive screening of T cell recognition against large libraries of patient-derived neoepitopes (12, 16–18). Here, we use DNA-barcode labelled pMHC multimers as a strategy to screen for CD8+ T cell recognition, using 151-585 predicted neoepitopes per patient, presented in a multimeric form in the context of patient-matched HLA-I molecules (19, 20). Using this strategy, we determine the presence of CD8+ T cells recognizing mutation-derived neoepitopes, here denoted as NeoAntigen Reactive T cells (NARTs), in the TIL Inf products from 26 patients with metastatic melanoma. Furthermore, we examined the persistence of such T cells in samples of peripheral blood collected at multiple time-points after therapy. This comprehensive mapping of NARTs demonstrates a substantial T cell reactivity level towards patient-derived neoepitopes and a positive influence on clinical outcome following TIL-ACT. This highlights the importance of detecting and enhancing the levels of such T cells in TIL-ACT.

26 Moreover, this study provides essential data to support efforts to identify the few immunogenic neoepitopes

27 that give rise to T cell recognition out of the large number of predicted neopeptides. Recent efforts have

28 been made to identify the parameters, which determine the immunogenicity of a given neoepitope (21) and

29 facilitate more accurate prediction of such sequences for therapeutic measures. In the current study, we

30 evaluated a total of 5921 predicted neopeptides, and identified T cell recognition towards 106 (1.8 %) of

31 these in TIL Inf products. Using this large data set, we further assessed the influence of HLA-binding,

32 antigen expression level, clonality, TMB, and type of mutation on immunogenicity (i.e. recognition of a

33 given neopeptide).

34 ## Results

35 **Identification of neoepitope-reactive CD8+ T cells**

36 In a cohort of metastatic melanoma patients treated with TIL adoptive cell transfer (Supplemental Table 1)

37 prediction of patient-specific mutated HLA-I epitopes was performed using WES and RNA sequencing on

38 tumor material and normal tissue PBMCs. The in silico neopeptide prediction platform MuPeXI

39 (http://www.cbs.dtu.dk/services/MuPeXI/) was employed to identify single nucleotide variants and in-

40 dels/frameshifts from the sequencing data specific to the cancer material (5, 20). Mutation-derived peptides

41 were subsequently ranked using netMHCpan (20, 22) and transcription of the corresponding gene (tran-

42 scripts per million (TPM)) (see methods) with the aim of including at least 200 neopeptides per patient.

43 We covered 30 different HLA alleles ranging from 2-6 HLA alleles per patient (avg. 4.4 HLAs) (Supple-

44 mental Figure 1, A and C), however, HLA-C*02:02 and C*05:01 were excluded from data analyses due to

45 technical concerns. Thus, the final neopeptide library ranged from 151-585 peptides per patient (Supple-

46 mental Figure 1B), with the most frequent alleles in our cohort being HLA-A*01:01 and C*03:04 (Supple-

47 mental Figure 1C). In addition to neopeptides, we also included a small set of known CD8 T cell epitopes

48 derived from common human viruses: EBV, CMV, and influenza virus (FLU). These represent 'bystander'

49 T cells in the TIL Inf product, and also serve as positive controls for the technical process.

50   DNA-barcode labelled neopeptide libraries were constructed as described previously (19) using UV-medi-

51   ated peptide-MHC exchange (23, 24) and fluorescent streptavidin-labelled dextrans (see methods). PBMCs

52   and TIL Inf products were stained with patient-specific multimer libraries followed by sorting of multimer-

53   binding CD8 T cells. The co-attached DNA-barcodes was amplified from the sorted T cell population to

54   reveal antigen specificity (19) (Figure 1A). We defined biologically relevant NARTs, as NARTs with an

55   estimated frequency of at least 0.01%, and without presence in partially HLA-matching healthy donor

56   PBMCs. To assess the reproducibility of our pMHC multimer library screens, we screened TIL samples of

57   nine patients twice with the same library demonstrating a correlation between technical replicates ($R =$

58   $0.55, p < 2.2 \cdot 10^{-16}$) (Supplemental Figure 1D).

59   An example of the analysis of enriched DNA barcodes and their corresponding pMHC in a TIL Inf product

60   from patient M22 (PR) is depicted in Figure 1B and for patients M14 (PD) and M26 (CR) in Supplemental

61   Figure 2. In patient M22, NARTs were detected for 3/4 HLA molecules included, although most reactivity

62   was seen against HLA-A*01:01 restricted peptides. Of interest, 7 HLA-A*01:01-restricted neoepitopes

63   recognized by the M22 TIL Inf product comprised the C-terminal amino acid sequence SILSY

64   (AKAP9^{P1796L}), and CD8+ T cells specific for each of these peptides were confirmed in TILs with single

65   tetramer staining (Supplemental Figure 3A).

66   From in silico structural models of the interaction between the different AKAP9^{P1796L} peptide variants and

67   the HLA-A*01:01 molecule, we observe that leucine (L), introduced by the mutation, protrudes from the

68   HLA binding groove for potential interaction with a TCR. Furthermore, the four 8-10mer epitope variants

69   share this conformation when bound to HLA-A*01:01 (Supplemental Figure 3B). This suggests that the

70   AKAP9^{P1796L} amino acid substitution has given rise to multiple neoepitopes that may be recognized by the

71   same population of CD8 T cells, but with different affinities. The binding affinity hierarchy can be assessed

72   both by the estimated frequency (Supplemental Figure 3C) and the MFI of the tetramer populations (Sup-

73   plemental Figure 3D) and indicates favorable interaction with the 9mer and 10mer neoepitopes holding the

74   SILSY motif.

75 Screening of TIL Inf products from 26 melanoma patients with personalized multimer libraries resulted in

76 the detection of 106 different NART populations across the cohort. NARTs were detected in 18 out of 26

77 TIL Inf products, ranging from zero to 13 NART populations per sample. To avoid any potential bias based

78 on differences in HLA coverage, the number and frequency of detected NARTs were normalized to the

79 average HLA coverage of the cohort (4.4 HLAs per patient). Following HLA normalization the median no.

80 of NARTs per TIL Inf product was 3.7 (range 0-12.1, Figure 1C, blue circles). Additionally, we detected

81 the presence of virus-specific CD8+ T cells towards a selected list of virus-derived epitopes in half of the

82 TIL Inf products (13 out of 26 patients, Figure 1C, red circles) which is in line with previous analyses of

83 TIL Inf products (25, 26). Across all TIL Inf products, we observed an estimated NARTs frequency of 0-

84 38.6% (median = 0.63%) out of total CD8+ T cells (Figure 1C).

85 **Recognition of melanoma tumor cells by NARTs in vitro**

86 The TIL Inf product from most patients (16 of 26), was previously analyzed for tumor recognition properties

87 in terms of cytokine secretion towards an autologous tumor cell line, generated from the same tumor biopsy

88 as the TIL Inf product (4). The estimated frequency of NARTs identified in this study correlated with the

89 capacity of the TIL Inf product to recognize the tumor, indicating that detected NARTs may indeed con-

90 tribute to tumor cell recognition (Figure 2A). While a significant association was observed, the effect on

91 cytokine secretion from other immune subsets, tumor antigens classes, or NARTs restricted to HLA-alleles

92 not included in our study cannot be excluded.

93 We additionally investigated the direct tumor recognition capacity of sorted and expanded neoepitope-spe-

94 cific T cell populations. From patient M22 TIL Inf product, we sorted USP34^{S1391F} – derived NLFR-HLA-

95 B*08:01-specific T cells using tetramers. The presence of such T cells was verified (3.2%, Figure 2B), and

96 post-sort expansion resulted in purity of > 96% (Figure 2C). The expanded NLFR-HLA-B*08:01-specific

97 T cells displayed tumor-recognition determined by cytokine secretion upon co-culture with an autologous

98 tumor cell line with (60.1%) and without (2.87%) pre-treatment with IFNγ (Figure 2D). Thus, tumor-recog-

99 nition was specific, and greatly enhanced by IFNγ pretreatment of the autologous tumor cell line. It has

100   previously been demonstrated that IFNγ pretreatment enhances MHC-I expression and antigen presentation

101   in both autologous (8) and established tumor cell lines (27). We also sorted CD8+ T cells specific to two

102   AKAP9^{P1796L} peptide variants followed by rapid expansion (Supplemental Figure 4A), which recognized

103   their respective AKAP9^{P1796L} variant (Supplemental Figure 4B). These sorted T cell populations, both rec-

104   ognized autologous tumor cell lines with and without pre-treatment with INFγ (Supplemental Figure 4C).

105   This indicates that some multimer-detected NARTs are capable of further expansion and can specifically

106   recognize autologous tumor cell lines.

107   **The number and frequency of NARTs is associated with the clinical outcome of TIL-ACT**

108   Next, we investigated whether higher diversity (number of responses) and frequency of NARTs in TIL Inf

109   products correlate with improved clinical efficacy of TIL-ACT. NARTs were detectable across all RECIST

110   groups, although they were severely depleted from TIL Inf products given to patients that developed pro-

111   gressive disease (n = 6) (Figure 3A). Overall, NARTs tended to demonstrate greater diversity in products

112   from responders compared to non-responders (Figure 3B).

113   The estimated NART frequency within TIL Inf products was significantly higher in responders compared

114   to non-responders (Figure 3, C and D, Supplemental Figure 5, A and B), suggesting that NART frequency

115   affects clinical outcome. Tumor mutational burden and number of predicted neoepitopes were uniformly

116   distributed across RECIST groups (Supplemental Figure 5, D and H), and no difference was observed be-

117   tween responders vs non-responders (Supplemental Figure 5, E and I). Tumor mutational burden was, how-

118   ever, associated with longer progression-free survival (Supplemental Figure 5F), as previously indicated

119   (5). Although, we do not observe a strong influence of the number of predicted neoepitopes on progression-

120   free survival (Supplemental Figure 5J).

121   Next, we investigated whether the diversity and frequency of NARTs within TIL Inf products affected

122   progression-free survival and overall survival. Patients in whom the number of NARTs was above the me-

123   dian of 3.7 ('High', n = 13) had an increased progression-free survival (p = 0.025, HR 2.62; %95CI = 1.05-

124   6.50) compared to patients below the median ('Low', n = 13) (Figure 3E). Likewise, patients with a high

125   NART frequency within TIL Inf products (median = 0.7%) ('High', n = 13) demonstrated significantly

126   improved progression-free survival (p = 0.026, HR 2.60; %95CI = 1.05-6.47) compared to patients with

127   low NART frequency ('Low', n = 13) (Figure 3F). High NART frequency also showed a positive effect on

128   overall survival (Supplemental Figure 6B); however, no such correlation was found with NART diversity

129   (Supplemental Figure 6A). Note, that overall survival might also be affected by subsequent treatment given

130   after TIL-ACT.

131   Interestingly, the clinical impact of NART frequency was most prominent for patients above the 66th per-

132   centile. For NART frequency, the 'High' patient group (above the 66th percentile, n = 9) showed signifi-

133   cantly longer progression-free survival (p = 0.0016) (Figure 3H) and overall survival (p = 0.021) (Supple-

134   mental Figure 6D) as compared to 'Intermediate' patients (equal to or below the 66th percentile and greater

135   than the 33rd percentile, n = 8) or 'Low' patients (equal to or below the 33rd percentile, n = 9). In contrast,

136   NART diversity did not significantly affect survival (PFS and OS) when comparing groups split by the 66th

137   and 33rd percentiles (Figure 3G and Supplemental Figure 6C). The 66th and 33rd percentiles corresponded

138   to a frequency of 3.26% and 0.03%, respectively, while the same percentiles for NART diversity were 5.65

139   and 0.88 NARTs, respectively.

140   In our analysis, T cell recognition of different overlapping peptides originating from the same mutation

141   were defined as multiple individual NART populations. However, T cell recognition of multiple neopep-

142   tides, could also arise from cross-reactivity of a single NART population towards several similar epitopes.

143   To avoid any bias in our data analyses based on such potential cross-reactive T cell populations, we reduced

144   the number of detected NART responses to the number of unique immunogenic somatic mutations recog-

145   nized by NARTs (median = 2.6), and redid our survival analysis using the most frequent NART as a proxy

146   for recognition of all overlapping epitopes from the same non-synonymous mutation. The result showed a

147 similar association: Both NART diversity and frequency correlated with increased PFS, whereas only fre-

148 quency correlated with an increased OS (Supplemental Figure 6, E-H), ensuring that contribution from T

149 cell recognition of overlapping epitopes did not bias our overall observation.

150 In summary, this data suggests that high frequency of NARTs positively affects therapeutic outcome fol-

151 lowing TIL-ACT.

152 **NARTs are detected in peripheral blood after TIL-ACT and decline over time**

153 As indicated by others (10, 28), an essential factor for TIL-ACT efficacy is the capacity of transferred T

154 cells to persist in patients following therapy. This can be measured based on their presence in peripheral

155 blood over time after transfer. For 19 patients, blood samples were available taken 8 days before TIL-ACT

156 and at different time points after TIL infusion, i.e., < 1 month after TIL-ACT, < 4 months after TIL-ACT,

157 < 12 months after TIL-ACT, < 24 months after TIL-ACT, and < 48 months after TIL-ACT (Supplemental

158 Table 1). NARTs present in the first or later PBMC samples post-ACT were defined as 'engrafted'. Fur-

159 thermore, if a given NART is detected in multiple later PBMC samples, that NART is regarded as persist-

160 ing. Each sample was screened for T cell-recognition towards neopeptides included in the full patient-

161 specific neoepitope-MHC library, exemplified by patient M22 (PR) (Figure 4A). In M22 only virus-specific

162 T cells could be detected in the Pre-ACT PBMC sample, namely, B*08:01-restricted FLU-ELR (v1), EBV-

163 RAK (v17), EBV-QAK (v30), and EBV-FLR (v31). These virus-specific CD8+ T cells were detectable

164 throughout most time points, while NARTs engrafted (PBMC < 1 month) and persisted in the following

165 PBMC samples up to one year after treatment.

166 Similar NART kinetics was observed in patient M45 (PR), with NARTs recognizing overlapping ne-

167 oepitope containing the mutated sequence SAGA (SORC2^{A1093S}) (Supplemental Figure 7). SORC2^{A1093S}

168 was first recognized in the M45 TIL Inf product, and immune recognition persisted in PBMCs until the last

169 recorded time point (< 12 months). Furthermore, M45 showed immune recognition towards the same ne-

170 oepitope DIHF (ZNF786^{M87I}) bound to multiple HLA alleles (HLA-A*01:01, A*24:02, and B*13:02).

171 Recognition of ZNF786^{M87I} was initially discovered in the TIL Inf product, and while it persisted on HLA-

172 A*24:02 until the last time point for M45, it appeared to incompletely persist on HLA-A*01:01 and

173 B*13:02. This overall suggests ZNF786^{M87I} to produce a promiscuous neoepitope capable of binding mul-

174 tiple HLAs with a preference for HLA-A*24:02. HLA promiscuity is otherwise known to occur for viral

175 epitopes (29).

176 The median NART diversity and frequency across RECIST categories were followed to assess the overall

177 kinetics of NARTs post- -ACT. Note, that most non-responders did not have PBMC samples for < 12

178 months and thereafter (7/10). NART diversity increases markedly when comparing pre-ACT PBMCs and

179 the TIL inf product, and declines over time post-TIL-ACT in the CR, PR and SD patient groups; displaying

180 the expansion of NART populations in the TIL Inf product and their persistence after therapy (Figure 4B).

181 NART frequency demonstrated similar kinetics to NART diversity. However, only responders appeared to

182 have substantial frequencies of NARTs within TIL Inf products (Figure 4C). Unlike the other groups, pa-

183 tients with progressive disease did not display any NARTs within TIL Inf products (n = 3); however, they

184 did appear to have ongoing NART recognition in peripheral blood before and after therapy, although at

185 lower frequencies (Figure 4, B and C).

186 Finally, we compared responders and non-responders in relation to NART diversity across all time points

187 and found that responders have a higher NART diversity in PBMCs collected before TIL-ACT (Figure 4D).

188 Similarly, we find an increased NART frequency in responders before TIL-ACT, within TIL Inf products,

189 and at early time points following infusion (> 1 month) (Figure 4E).

190 In conclusion, we observed a broad repertoire of NARTs recognizing single neoepitopes, overlapping ne-

191 oepitopes, and HLA promiscuous neoepitopes in TIL Inf products of metastatic melanoma patients treated

192 with TIL-ACT. These NARTs show signs of engraftment and can persist in peripheral blood after TIL-

193 ACT. Furthermore, we observe that responders have a higher estimated NART frequency before and fol-

194 lowing TIL-ACT in peripheral blood supporting prior prospective efforts (30).

Engrafted neoepitope-specific CD8 T cells dominate immune recognition in responders of TIL-ACT

To better understand the dynamic relationship between pre-existing, ongoing and TIL-derived immune recognition, we annotated each detected NART according to their first appearance from 8 days prior to therapy (pre-ACT PBMCs) to the last available time point. Thus, if a NART population appeared exclusively in pre-ACT samples, it was annotated "Pre-ACT". If a given NART was detected in both pre-ACT PBMCs and in the given TIL Inf product, it was denoted "Pre/TIL", while if it first appeared in the infusion product it was denoted "TIL". Finally, if a NART population first appeared in a later PBMC sample it was regarded as "novel" annotated with its first time of appearance and followed from there on out (see patient overview in Supplemental Figure 8).

Using this categorization, we observed that persisting NARTs derived from the TIL Inf product (Pre/TIL + TIL) were present across responders and patients with stable disease at multiple time points after infusion, but absent in patients with progressive disease (Figure 5, A and B, Supplemental Figure 8). Additionally, we observe that 7/8 responders and 5/10 non-responders with available pre-ACT material had pre-existing NARTs (Pre-ACT + Pre/TIL). Pre-existing NARTs are likely clinically relevant as TIL Inf products from responders were overall dominated by pre-existing immune recognition that was further expanded to high frequencies within the TIL Inf product (Pre/TIL) (Figure 5B, Supplemental Figure 8). Mind however, that the presence of pre-existing NARTs that were further expanded did not appear sufficient to generate a clinical response as we also observed Pre/TIL NARTs in 3 patients with stable disease (Supplemental Figure 8). The perceived therapeutic benefit of pre-existing NARTs that were further expanded may therefore relate more to the high frequency and persistence after expansion in selected patients, than to their presence alone.

We observed that 62.5% (60/96) of NARTs observed in TIL Inf products were also detectable post-ACT (Figure 5C). Furthermore, 57% of NARTs detected post-ACT were novel, and did not originate from the TIL Inf product (80/140), whereas 43% originated from the TIL Inf product (60/140) (Figure 5C). These

11

219 novel NARTs were transiently appearing and could represent epitope spreading. However, their appear-

220 ances may not necessarily have therapeutic benefit, as they were observed across all RECIST groups (Fig-

221 ure 5, A and B), and present at lower frequency than newly engrafted NARTs (TIL NARTs present in post-

222 ACT PBMCs) (Figure 5D). Finally, we observe that engrafted NARTs derived from the TIL Inf product

223 (TIL + Pre/TIL) had a higher estimated frequency compared to their non-engrafted counterparts in the TIL

224 Inf product (Figure 5E) suggesting engraftment to be associated with prior frequency.

225 To evaluate the impact of engrafted NART populations separately from non-engrafted and novel NARTs,

226 appearing only in TIL Inf products and post-ACT PBMCs, respectively, we compared the diversity and

227 frequency of engrafted NARTs (Pre/TIL and TIL) in responders and non-responders with available PBMCs

228 throughout all time points (Figure 5, F and G). Interestingly, we observe that non-responders had a markedly

229 lower diversity (Figure 5F) and frequency (Figure 5G) of engrafted NARTs compared to responders in the

230 first two sampling time-points post-ACT (< 1 month and <4 month). These data suggests that responders

231 were treated with TIL Inf products characterized by high frequent, engrafting NARTs, where non-respond-

232 ers were treated with TIL Inf products containing a relatively lower frequency of NARTs that were unable

233 to engraft and persist post-ACT. This is in line with prior TCR sequencing efforts (28).

The characteristics of immunogenic neoepitopes

235 Based on the large screen presented here, we evaluated T cell recognition against 5921 predicted neopep-

236 tides that were selected based on their HLA binding characteristics and gene transcriptional level in tumor

237 NGS data. Of these predicted neopeptides, we detect specific CD8+ T cell recognition towards 204 ne-

238 oepitopes in either TIL Inf products or PBMC samples from melanoma patients, while the remaining 5717

239 were not recognized by T cells in the evaluated patients (Figure 6A). The pool of immunogenic neoepitopes

240 displays similar characteristics related to both clonality and C/T mutations as the total library of evaluated

241 neopeptides (Figure 6A). Hence, we do not observe a specific enrichment of T cell recognition towards

242 clonal mutations as has previously been suggested for NSCLC (31). Interestingly, cancer driver genes (32)

243 are significantly overrepresented in the fraction of immunogenic neoepitopes compared to the fraction of

244   non-immunogenic neopeptides (Figure 6A, 6.5% vs. 3.3%, p = 0.0043). However, we do not find any im-

245   munogenic neoepitopes to be shared among patients, as has previously been observed in TILs isolated from

246   colorectal cancer (33).

247   Our neopeptide library was preselected for predicted HLA binding. Within this pool, neoepitopes can be

248   classified as either 'conserved binders' (CB, i.e., neopeptides with similar HLA binding as the mutated

249   peptide versus the germ-line sequence) or 'improved binders' (IB, where the mutation affects HLA binding

250   capabilities resulting in a neopeptide with improved HLA affinity compared to the germline sequence) and

251   defined in Bjerregaard, et al. (34) (Figure 6B). Immunogenic neoepitopes were represented in both catego-

252   ries, and we did not observe a significantly different distribution of immunogenic versus non-immunogenic

253   neopeptides among conserved versus improved binders (3.4% CB vs. 3.5% IB, p-value = 0.99, Figure 6B).

254   Furthermore, within the selected HLA affinity range evaluated here, we did not observe any further impact

255   of HLA %rank score on neopeptide immunogenicity, evaluated as the potential enrichment of immunogenic

256   neoepitopes < %rank = 0.5 (p = 0.71, z-test, Figure 6C).

257   In line with previous findings (33), we observed an enrichment of genes with RNA expression > 2 TPM

258   among immunogenic neopeptides (Figure 6D, p = 0.001, z-test).

259   TMB and predicted neoepitope load have previously been demonstrated to be predictive for TIL-ACT out-

260   come (5). We find a strong correlation between TMB and number of predicted neoepitopes (Supplemental

261   Figure 9A). However, we do not find a correlation between TMB or the number of predicted neoepitopes

262   to NART diversity and NART frequency (Supplemental Figure 9, B-E). This indicates that the presence of

263   NARTs in TIL Inf products is an independent marker of therapeutic outcome in patients with metastatic

264   melanoma. Since the inter-patient variation in neopeptide library size may affect the correlation, we also

265   correlated the number NARTs detected and estimated frequency within the top 151 predicted neoepitopes

266   to have an equal representation of all patients (Supplemental Figure 9G). Again, no strong correlation was

267   evident (Supplemental Figure 9, H-K), as multiple patients with low TMB showed medium sized popula-

268   tions of neoepitope-specific CD8 T cells in their respective TIL Inf product (Supplemental Figure 9L). This

269   emphasizes the need to improve our predictive capacity for identification of those neoepitopes that give rise

270   to functional T cell recognition and tumor cell killing, and furthermore highlight that other parameters,

271   beyond TMB, impacts immune recognition.

272   The tumor microenvironment has a substantial influence on the capacity to generate a T cell response to-

273   wards the tumor and for such T cells to exert their function. Although the generation of TIL Inf products is

274   conducted in vitro, the tumor microenvironment may still affect the capacity for T cell expansion and func-

275   tion. We used the available transcriptomic data from our neoepitope prediction pipeline as input for a dif-

276   ferential gene expression analysis, grouping patients according to higher or lower than median sum of esti-

277   mated NART frequency within TIL Inf products. From this we observe 226 differentially expressed genes

278   (Figure 6E), which are associated with 383 enriched gene ontology (GO) gene sets (35). The top 20 enriched

279   GO gene sets were a collection of humoral and B-cell mediated mechanisms and several pathways pertain-

280   ing to the immune cell signal transduction (Supplemental Figure 10). These gene sets are highly relevant

281   in light of the recently revealed relationship between intratumoral lymphoid structures, antigen-presenta-

282   tion, and therapeutic benefit following immunotherapy (36). Of further interest, we observe enriched pres-

283   ence of GO terms relating to lymphocyte-mediated immunity (Figure 6F) and increased T-cell proliferation

284   (Figure 6G).

Discussion

285

286   Immune-recognition and tumor killing by cytotoxic T cells are associated with a positive outcome across

287   multiple immunotherapies (9, 31, 37), however, the presence of neoepitope-specific CD8+ T cells in TIL-

288   ACT remains incompletely documented outside case responders (10–15). In the present study, we investi-

289   gated the capacity of TIL Inf products to recognize predicted, HLA-binding neoepitopes originating from

290   expressed, non-synonymous mutations from 26 patients with metastatic melanoma. To this end, we utilized

291   DNA barcode-labelled pMHC multimers wherefrom we quantified NART diversity and frequency in TIL

292   Inf products and patient PBMCs. We report recognition of a total of 106 neoepitopes within TIL Inf prod-

14

293 ucts from this cohort across all 4 RECIST groups. Supporting that the presence of NARTs affects the clin-

294 ical response to TIL-ACT, we found that NART diversity and frequency is significantly lower in patients

295 with PD when comparing to patients with SD and PR, and that NART frequency correlates with PFS and

296 is significantly higher in patients with clinical response to TIL-ACT (CR+PR).

297 We find that both NART diversity and frequency is highly variable across RECIST groups; especially

298 within responding patients: 3 out of 11 CR/PR patients had zero detectable NART populations. This varia-

299 bility could be due to limitations in neoepitope selection, contribution from other antigen types, insufficient

300 HLA coverage, sampling bias or NART response frequencies below the threshold for detection (i.e. result-

301 ing in false negative detection), or other NART-independent and/or HLA-I independent pathways such as

302 the MR1-dependent immune recognition pathway (38).

303 Following each NART population from first appearance to last available PBMC time point further uncov-

304 ered, that responders were characterized by circulating NARTs of higher diversity and frequency in pre-

305 treatment PBMCs. This is interesting, because pretreatment circulating NARTs could represent a biomarker

306 for ongoing tumor recognition by CD8 T cells, which, in extension, could provide a non-invasive way to

307 measure immune activity of the tumor. However, identification of NARTs is a laborious and patient specific

308 process, and for biomarker purposes a simpler measurement of NART reactivity should be developed. Re-

309 sponders were furthermore predominantly treated with TIL Inf products of high NART frequency capable

310 of engrafting and persisting after TIL-ACT at an estimated frequency higher than 0.01%. Additionally, we

311 observe that engrafted NARTs initially appeared with an overall higher estimated frequency in the TIL Inf

312 product compared to non-engrafted NARTs, which indicates that successful NART expansion precedes

313 successful engraftment. As mentioned, the persistence of tumor antigen-specific TCRs has been hypothe-

314 sized to drive therapeutic benefit following TIL-ACT (28). Interestingly, this hypothesis has recently been

315 supported in the metastatic melanoma setting (39), where the persistence of neoantigen-specific TCRs

316 post-TIL-ACT correlates with CD39-CD69- stem- like T cells capable of self-renewal, differentiation, and

317 further expansion upon stimulation. Future efforts to discover and quantify the presence of NARTs may

318   benefit from a simultaneous characterization of stem-like phenotypes to increase our understanding of why

319   certain NARTs are superior in their capacity for expansion and persistence. Together with our current re-

320   port, this identifies an unmet need to improve the manufacturing of TIL Inf product to increase the fre-

321   quency of tumor-specific CD8 T cells that are able to engraft and persist in patients post-ACT.

322   Interestingly, we observed that 2 out of 3 patients with PD and multiple patients with SD appeared to have

323   NARTs in peripheral blood despite the lack of persisting NART populations in the TIL Inf product. This

324   suggests that selected non-responders have ongoing tumor recognition, that wasn't expanded by the TIL

325   manufacturing process (i.e. failure to expand meaningful NARTs) perhaps due to poor tumor immune in-

326   filtration (i.e. immunologically "cold"). Thus, development of technologies to expand tumor-specific CD8

327   T cells from peripheral blood may be beneficial for the future treatment of patients that do not benefit from

328   conventional TIL-ACT. Given information on the antigen recognized in peripheral blood, other strategies

329   such as therapeutic vaccination (40, 41) could furthermore be combined to increase the likelihood of gen-

330   erating long-lasting CD8 and CD4 memory T cells from TIL-ACT.

331   We additionally observed novel NARTs at multiple time points post infusion in both responders and non-

332   responders. This might illustrate epitope spreading as a result of tumor cell killing in responders. However,

333   these late-emerging NART populations are present at a lower frequency and appear to be more transient

334   than those transferred in the TIL Inf product. Thus, epitope-spreading, with T cell recognition of pre-exist-

335   ing mutations and their derived peptide products does not appear to play a major role following TIL-ACT.

336   However, this does not exclude a potential therapeutic role for epitope-spreading based on T cell recogni-

337   tion towards novel mutations occurring after immunotherapy.

338   Finally, we observe that lymphocyte activity and proliferation within the tumor microenvironment is asso-

339   ciated with higher NART frequency in TIL Inf products, suggesting that ongoing immune activity within

340   the tumor supports the manufacturing of TIL Inf products containing a high frequency of NARTs. Superior

341   T cell proliferation and response to checkpoint inhibition is associated with intratumoral tertiary lymphoid

342   structures, which maintain a niche of professional antigen-presenting cells and proliferating T cells (36,

16

343   42). Tertiary lymphoid structures could, therefore, possibly support the successful expansion of TILs prior

344   to successful TIL-ACT. However, the relationship between ongoing T cell proliferation, successful TIL

345   expansion and therapeutic response remains undetermined.

346   Both TIL expansion and post-transfer persistence of CD8 NARTs may additionally be affected by support-

347   ing CD4 T cells (43). So far, no differences has been observed between CD8 enriched TIL products and

348   TIL products containing different lymphocytes (although the majority are CD8) (44). Furthermore, epitope

349   spreading as evaluated here for CD8 T cell may likewise occur for CD4 T cells, and the further insight to

350   the relationship between CD4 and CD8 tumor reactive T cells and the relevance for shared antigen recog-

351   nition are critical aspects to address for future improvements of immunotherapy. However, technical limi-

352   tation are still prohibiting a detailed epitope mapping of CD4 NARTs, as conducted here for CD8 NARTs

353   (45).

354   In this study, we screened for recognition among 5921 predicted neopeptides arising from non-synonymous

355   mutations, of which we find recognition to 1.8% (106 neoepitopes) in TIL Inf products, and additionally

356   98 neoepitopes in peripheral blood before or after TIL infusion, making a T cell recognition percentage of

357   3.4%. This illustrates that neoepitope prediction is feasible, but it remains a cumbersome approach to iden-

358   tifying neoepitope-specific CD8+ T cells in metastatic melanoma. While recent efforts have led to signifi-

359   cant improvements in the prediction of antigen processing and HLA binding (46), a gap remains in our

360   ability to predict which of the presented neoepitopes are able to give rise to T cell recognition (21). Among

361   the neoepitopes recognized by T cells in this study, we observed an enrichment of neoepitopes derived from

362   cancer driver genes and genes expressed above 2 TPM. However, despite these characteristics, the majority

363   of the neoepitopes detected was derived from passenger mutations, and no stringent criteria could be as-

364   signed to determine the neoepitopes driving T cell recognition.

365   In conclusion, our study describes the critical contribution of NARTs to the clinical outcome in TIL-ACT

366   therapy and provides a thorough characterization of neoantigens recognized by T cells in this therapeutic

367   context. To this end, our study highlights a significant need for improving TIL-ACT manufacturing and the

368 capacity to predict immunogenic neoepitopes. Strategies to improve the expansion and engraftment of

369 NARTs in TIL Inf products should further improve the clinical outcome.

Methods

370

Patient material

371

372 To study the role of NARTs in TIL-ACT in melanoma, we evaluated 26 patients with unresectable or met-

373 astatic melanoma enrolled in a phase I/II clinical study of adoptive cell transfer, ClinicalTrials.gov Identifier

374 NCT00937625. Demographic and clinical information for each patient ID are available in previous reports

375 (4, 5, 26). TIL Infusion (Inf) products were generated by expanding TILs in vitro from tumor lesions fol-

376 lowing a rapid expansion protocol (REP) with high-dose IL-2, as described previously (47). All patients

377 were included at the time of progression from previous treatment(s) with either IL-2/IFNα and/or anti-

378 CTLA-4 treatment and/or DC vaccination and/or Temozolomide and/or Vemurafenib (26). Furthermore,

379 as specified previously, four patients received Vemurafenib between surgical resection and TIL-ACT (M27,

380 M29, M35, M36) (4). Clinical response was assessed according to RECIST 1.0. Among the 26 patients,

381 five were complete responders (CR), six were partial responders (PR), ten were stable disease (SD), and

382 five were progressive disease (PD) patients (4), with a median progression-free survival (PFS) and overall

383 survival (OS) of 3.85 and 23.25 months, respectively. Using DNA-barcode-labelled pMHC multimers, we

384 analyzed the TIL inf products from all 26 patients for neoepitope-specific CD8+ T cells. From 19 of these

385 patients, we additionally analyzed corresponding PBMC samples before and at multiple time points after

386 TIL ACT (Supplemental Table 1). Tumor sequencing data (RNA and WES) was available from 26 of the

387 27 patients enrolled in the trial.

388 PBMCs from healthy donors were obtained from whole blood by density centrifugation on Lymphoprep in

389 Leucosep tubes and cryopreserved at −150◦C in fetal calf serum (FCS, Gibco) + 10% DMSO.

390 **TIL sorting and expansion.** Young TILs were thawed and cultured overnight at 37°C in Complete Me-

391 dium (CM, RPMI-1640 supplemented with 10% heat-inactivated human serum), 100 U/ml penicillin, 100

392 µg⁄ml streptomycin, 1.25 µg/ml Fungizone and 6,000 IU⁄ml Interleukin 2. Cells were washed twice in R0

393 (RPMI-1640, 100 U/ml penicillin, 100 µg⁄ml streptomycin) and stained with 0.2 µg of in-house produced

394 pMHC tetramers conjugated to PE, APC or BV421 for 10 minutes at 37°C constructed using empty disul-

395 fide-stabilized monomers where possible (A*02:01-Y84C) (48). Anti-CD4-FITC and anti-CD8-PerCP an-

396 tibodies were added for a further 20 minutes at 37°C. Cells were washed with R0 and resuspended in R0 +

397 10% heat-inactivated human serum and sorted by flow cytometry using the BD FACS Aria cell sorter (BD

398 Biosciences, San Jose, CA, USA) into a 96-well plate. Sorted CD8+ tetramer+ cells were expanded 9 + 9

399 days in two sequential mini-rapid expansions (dependent on sorted cell numbers). In brief, 5×10^5 allogeneic

400 feeder cells from healthy donors, 30 ng/ml OKT3 antibody (anti-CD3, Janssen-Cilag), master mix made of

401 50% CM and 50% rapid expansion medium (RM) consisting of AIM-V medium (Gibco) and 1.25 µg⁄ml

402 Fungizone supplemented with 6,000 IU⁄ml IL-2 with 10% HS were added to sorted cells and cultured at

403 37°C. 50% of the media (without OKT-3) was replaced after five days and subsequently every two days.

404 **Intracellular Cytokine Assay.** Tumor cells were either pretreated with interferon-γ (IFNγ) (100 IU/ml,

405 Peprotech, London, United Kingdom) or left untreated for three days. TILs were then added in a 1:1 ratio,

406 with protein transport inhibitors Brefeldin A (1:1000 dilution, GolgiPlug™, Cat No 555029, BD),

407 Monensin (1:1000 dilution, GolgiStop™, Cat No 554724, BD), and anti-CD107a-BV421 antibody (Clone

408 H4A3, BD 562623). Tumor cells and TILs were co-cultured for 5 hours, after which all cells were stained

409 with Near-IR Live/Dead (Life Technologies) and for surface markers CD3-FITC, (Clone SK7, BD 345764),

410 CD8-QDot605 (Clone 3B5, Thermo Fisher Q10009), CD4-BV711 (Clone SK3, BD 563028). Subse-

411 quently, the cells were fixed and permeabilized (eBioscience) overnight and stained for intracellular cyto-

412 kines TNF-APC (Clone MAb11, BD 554514) and IFN-γ-PE-Cy7 (Clone B27, BD 557643). Cells were

413 analysed on a Novocyte Quanteon (ACEA Biosciences). See details related to antibodies used in Supple-

414 mental Table 2.

415 **Neoepitope prediction.** WES and RNAseq data were obtained from digested tumor fragments except for

416 M22 and M24 where autologous tumor cell lines were used. Two WES files from M15 were utilized and

417   their results combined; one from autologous tumor digest another from an autologous tumor cell line. All

418   WES data were obtained from tumor material from the same biopsy as was used for manufacturing of the

419   corresponding TIL Inf products, expect for M22 where the tumor cell line was derived from an earlier time

420   point. FASTQ files from WES and RNAseq were pre-processed using Trim Galore (49) version 0.4.0. WES

421   reads were aligned to the human genome (GRCh38) using Burrows-Wheeler Aligner (50) version 0.7.15

422   with default mem parameters, and duplicate reads were marked using MarkDuplicates from Picard-tools

423   (51) version 2.9.1. Peptides were extracted and prioritized using MuPeXI (20) version 1.1.3 and

424   netMHCpan version 4.0 (22) providing as input the somatic variants obtained following GATK version

425   3.8.0 best practices, the RNAseq expression values calculated using Kallisto version 0.42.1 (52) and the

426   HLA alleles inferred from normal WES samples using OptiType version 1.2 (53). For patients with high

427   neoantigen load, all predicted neoepitopes with %rank ≤ 0.5 and TPM ≥ 0.1 were included. For patients

428   with lower neoantigen load, we lowered the expression threshold to ≥0.01 TPM, and selected top 200 pre-

429   dicted neopeptides according to %rank. All predicted neopeptides and virus control peptides were synthe-

430   sized and purchased from Pepscan (Pepscan Presto, The Netherlands) and dissolved to 10 mM in DMSO.

431   For each cancer-specific non-synonymous mutation, the HLA-I binding potential of mutation-derived pep-

432   tides was predicted using netMHCpan v 4.0 (20, 22). For each patient, a minimum of 200 top-ranking

433   neopeptides were included. The ranking was based on the predicted HLA-I binding (%rank) and the tran-

434   scription of the corresponding gene, as RNA Transcripts per Million (TPM).

435   **Clonality.** Copy number, purity and ploidy are found using Sequenza version 3.0 (54). As input, printed

436   reads from normal and tumor are used as input to Sequenza. Sequenza-utils version 3.0 bam2seqz with

437   GRCh38 as reference. To run the Sequenza copynumber call with GRCh38, the R packages

438   Shixiang/copynumber version 1.26.0 (55) is applied. The created seqz files are used as input to sequenza-

439   utils seqz_binding, the outputs are used to Sequenza utils snp2seqz. To reduce the amount of false negative

440   according to the bulid-in mutations called from Sequenza, copynumber files from the mutect2 output are

441   merged with the copynumber call from the bam files. Sequenza results and PyClone inputs are generated

442   with the Sequenza packages in R, version 3.6.1. To find clonal mutations, PyClone version 0.13.0 (56) is

443   applied with the cellularity given from Sequenza and max cluster of 30 and minimum size of 0 to get all

444   possible mutations given. Clonal mutations are filtered with a cluster size of minimum 80 and cellularity of

445   minimum 90. Clonality could not be computed for M22, M24 and part of M15 as the underlying WES data

446   came from autologous tumor cell lines.

447   **Generation of DNA-barcode labelled pMHC multimers.** Oligonucleotides containing distinct 25mer nu-

448   cleotide sequences (57) were purchased from LGC Biosearch Technologies (Denmark). All oligos carry a

449   6-nt unique molecular identifier (58). Oligonucleotides modified with a 5′ biotin tag (oligo A) were joined

450   to unmodified, partially complementary oligonucleotides (oligo B) to generate > 1000 unique double-

451   stranded AxBy DNA barcodes. Combinations of A and B oligos (one of each) were mixed with $5 \times$ Se-

452   quenase Reaction Buffer mix (PN 70702, Affymetrix) to final concentrations of 26 μM (Oligo A) and 52

453   μM (Oligo B), respectively; heated to 65°C for 2 min; and allowed to anneal by cooling slowly to < 35 °C

454   over 15–30 min. The annealed oligo As and Bs were elongated to create double-stranded AxBy DNA bar-

455   codes by adding Sequenase polymerase (70775Y, Affymetrix), 20 μM DTT and 800 μM or 72 μM dNTPs,

456   followed by incubation for 5–10 min at room temperature. Elongated AxBy barcodes were diluted in nu-

457   clease-free water + 0.1% Tween to 2.17 μM (with respect to the A oligo) and stored at −20°C. Attachment

458   of 5′ biotinylated AxBy DNA barcodes to PE- and streptavidin-conjugated dextran (Fina Biosolutions,

459   USA) was performed by mixing the two components at final concentrations of 14×10^{-8} M dextran back-

460   bone and 2.8×10^{-5} M barcode in order to obtain 0.5-2 barcodes for each dextran backbone and subsequent

461   incubation for 30 min at 4°C.

462   Refolded, biotinylated pMHC-I were subsequently added at a stoichiometry of approximately 16.5 pMHC

463   molecules per dextran, these were generated through UV-mediated exchange of cleavable ligands as de-

464   scribed previously (23, 24). In brief, MHC monomers bound to UV-sensitive ligands were mixed with

465   HLA-matching peptides at a final concentration of 50 μg ml−1 monomer and 100 mM peptide and exposed

466   to UV light for 60 minutes (366 nm). Afterwards, pMHC monomers were centrifuged for 5 min at 3300×g

467 and then coupled to DNA barcode- and PE-labeled dextran backbones to a final concentration of 35 µg

468 ml−1 monomer and 4.2 × 10−8 M barcode- and PE-labeled dextran backbone and incubated for 20 min on

469 ice. Then, a freezing buffer was added to reach PBS + 0.5% BSA + 100 µg mL−1 herring DNA + 2 mM

470 EDTA + 5% glycerol and 909 nM D-biotin and after 20 min on ice, the pMHC multimers were stored at

471 −20°C until use.

472 **T cell staining with barcode-labeled pMHC multimers.** Cryopreserved cells were thawed, washed twice

473 in RPMI + 10% FCS and then washed in barcode-cytometry buffer (PBS + 0.5% BSA + 100 µg mL−1

474 herring DNA + 2 mM EDTA). Before staining, MHC multimers were thawed on ice, centrifuged for 5 min

475 at 3300×g, and 1.5 µl (0.043 µg) of each distinct pMHC was taken from each well, avoiding potential

476 aggregates in the bottom, and pooled. The volume of the reagent pool was reduced by ultrafiltration to

477 obtain a final volume of ~ 80 µL of pooled MHC multimers per staining. Centrifugal concentrators (Vi-

478 vaspin 6, 100,000 Da, Sartorius) were saturated with BSA before use. Following ultrafiltration, the pool of

479 multimers was spun at 10.000×g for 2 min to sediment potential aggregates. An aliquot of ~ 5 µl of the

480 MHC multimer reagent pool was stored at −20°C for later baseline analysis. Prior to staining with the MHC

481 multimers, 50 nM dasatinib was added to up to 10×10^6 cells. The MHC multimer pool was then added to

482 the cells and cells were incubated for 15 min at 37°C in a total volume of 80 µl. Following incubation, the

483 cells were stained with an antibody mix containing CD8-BV480 (clone RPA-T8, BD 566121), dump chan-

484 nel antibodies (CD4-FITC (clone SK3, BD 345768), CD14-FITC (clone $M\varphi$P9, BD 345784), CD19-FITC

485 (clone 4G7, BD 345776), CD40-FITC (clone LOB7/6, Serotech MCA1590F), and CD16-FITC (clone

486 NLP15, BD 335035)), and a dead cell marker (LIVE/DEAD Fixable Near-IR; Invitrogen L10119) and

487 incubated for 30 min at 4 °C. Samples were stained with antibodies in 100 µL according to Supplemental

488 Table 2. Cells were washed three times in barcode-cytometry buffer and fixed in 1% paraformaldehyde

489 (PFA) for 0.5–24 h before they were washed twice and resuspended in barcode-cytometry buffer. Cells

490 were acquired within a week after multimer staining.

Sorting of pMHC multimer+ T cells. Multimer-binding CD8+ T cells were sorted on a FACS Aria Fusion or FACS Melody Cell Sorter (BD) into BSA saturated tubes containing 100 µl of barcode-cytometry buffer. We gated on single, live, CD8+, and dump channel (CD4, CD14, CD16, CD19, and CD40)-negative lymphocytes and sorted all multimer-positive PE cells within this population. As tested and described in Bentzen et al., inclusion of CD8+, multimer negative cells in the sorting gate does not have an impact on the final results because the fluorescence signal is used only for sorting out the relevant cells. Determination of antigen specificity is done solely based on the DNA barcode. The sorted cells were centrifuged for 10 min at 5000 g and the buffer was removed. The cell pellet was stored at −80 °C in a minimal amount of residual buffer (< 19 µL). %Multimer+ CD8+ T cells was used as input for estimation of epitope-specific CD8+ T cells (see Processing of DNA barcode sequencing data), 3 samples were run without exported flow cytometry files precluding adequate estimation of frequency after sequencing of DNA-barcodes (M15 TIL Inf product, M40 pre-ACT PBMCs, and M40 PBMCs < 1 month). TIL Inf product from M47 were stained again to estimated %multimer+ CD8+ T cells. M15 had no significant hits among barcoded multimers (i.e. sum of estimated frequency was set to 0%). See details antibody assay details in Supplemental Table 2.

DNA barcode amplification. DNA barcode amplification was performed using Taq PCR Master Mix Kit (Qiagen, 201443) and 3 µM of forward and reverse primers (LGC Biosearch Technologies). PCR amplification was conducted on sorted multimer-binding T cells (in < 19 µL of buffer) and on a triplicate of the stored aliquot of the MHC multimer reagent pool (diluted 10.000× in the final PCR) under the following conditions: 95°C 10 min; 36 cycles: 95°C 30 s, 60°C 45 s, 72°C 30 s, and 72°C 4 min. The multimer reagent pool was used as the baseline to determine the number of DNA barcode reads within a non-processed MHC multimer reagent library. PCR products were purified with a QIAquick PCR Purification kit (Qiagen) and the amplified DNA barcodes were sequenced at Primbio (USA) using an Ion Torrent PGM 316 or 318 chip (Life Technologies).

Processing of sequencing data from DNA barcodes. Sequencing data were processed by the software package "Barracoda", available online at (https://services.healthtech.dtu.dk/service.php?Barracoda-1.8).

516   This tool identifies the barcodes used in a given experiment assigns in PCR used sampleIDs and pMHC

517   specificity to each barcode, and counts the total number (clonally reduced) reads for each DNA barcode.

518   Furthermore, it accounts for barcode enrichment based on methods designed for the analysis of RNA-seq

519   data, implemented in the R package edgeR: specifically, log2 fold changes in read counts mapped to a given

520   sample relative to the mean read counts mapped to triplicate baseline samples are estimated using normal-

521   ization factors determined by the trimmed mean of M-values method. Barcodes with a log2 fold change

522   with a $p < 0.001$, which equals a FDR< 0.1 (estimated using the Benjamini–Hechberg method). Barracoda

523   outputs were further processed and annotated using R 4.0.2 - adding relevant clinical information, and

524   excluding signals arising from insufficient read depth (%read count < 0.1). Furthermore, biologically rele-

525   vant barcode enrichment was defined as an estimated frequency $\geq 0.01\%$, and without presence in partially

526   HLA-matching healthy donor PBMCs. 227 multimers were excluded due to technical concerns regarding

527   HLA-C*05:01 (M22, 140 multimers; M27, 46 multimers) and HLA-C*02:02 (M43, 41 multimers). Peptide

528   missannotations were also excluded, which originated from pipetting errors discovered through cross-ref-

529   erencing of ordering and annotation tables (M27, 1 multimer; M35, 40 multimers; M46, 1 multimer). Fre-

530   quency of a pMHC-specific CD8+ T cell population was estimated based on the %read count of the asso-

531   ciated barcode out of the total %multimer-positive CD8+ T cells population. Sum of estimated frequency

532   represents the pooled frequencies of all T cell populations in a given sample. Due to differences in number

533   of producible HLA molecules, number and frequency of neoepitope-specific CD8+ T cells were normalized

534   to the mean absolute HLA coverage in the cohort (average HLA covered (across all panels) / HLA covered

535   (patient panel)).

536   **Structural analysis of overlapping mutated peptides and the HLA binding.** Structural pMHC models

537   were generated using the method described in TCRpMHCmodels (59). All peptides were bound to HLA-

538   A*01:01 and the sequence for this MHC molecule was downloaded from the IMGT database (60). To get

539   the electrostatic potential for each of the pMHC models hydrogen atoms were added using the phenix.re-

540   duce protocol from (61) after which Delphi (62) was used to calculate the electrostatic potential with the

541   following parameters, scale=1.0, perfil=70.0, indi=4.0, exdi=80.0, prbrad=1.4, salt=0.15, ionrad=2.0, bnd-

542   con=2, linit=800, maxc=0.0001, sigma=2.0, srfcut=20.0 and gaussian=1. The electrostatic potential from

543   Delphi was finally virtualized using PyMOL (https://pymol.org/).

544   **Differential expression analysis.** RNAseq data for differential gene expression analysis exclusively came

545   from tumor digests i.e. no autologous tumor cell lines were used. Output files from Kallisto are used as

546   input to DESeq2 version 1.26.0 from R/biocinductor with default options(63) to find differential expressed

547   genes (adjusted p-values < 0.05, related to high and low sum of estimated frequency split by the median

548   and PFS split by equal or below the median). GO enrichment analysis was performed using R version 4.0.2

549   with the packages; enrichplot version 1.11.0.991 (64) and clusterProfier version 3.16.1 with Benjamin

550   Hochberg at p value adjustment (35).

551   **Statistics.** Statistical analysis of DNA barcoding data was performed using the software package "Barra-

552   coda" as described above. Survival analysis used percentiles and medians (number of NARTS or frequency)

553   to define thresholds to split the cohort. Any values matching the threshold were treated as belonging to the

554   lower group. Mantel-Cox test was used to evaluate the effect of NARTs on survival, and hazard ratios were

555   calculated using log rank-approach using Graph Pad Prism 8. Correlations were tested using non-paramet-

556   ric, two-sided Spearman correlation test, except in Supplemental Figure 1D, where we used a two-sided

557   Pearson correlation. Two-sided z-test (prop.test) was applied where specified in Figure 6A, C and D. All

558   two-group comparisons were performed using non-parametric Mann-Whitney test with a significance

559   threshold of 0.05. Multi-group comparisons were performed by an initial non-parametric Kruskal-Wallis

560   test followed by post hoc Dunn's multiple comparison test.

561   **Study approval.** This study was conducted using TILs and PBMCs from patients enrolled in the clinical

562   study: ClinicalTrials.gov Identifier NCT00937625. All patients signed a written consent form according to

563   the Declaration of Helsinki. The study was approved by the local ethics committee for the capital region of

564   Denmark (RegionH). Likewise, healthy donor samples were collected by approval of the local Scientific

565   Ethics Committee for the capital region of Denmark (RegionH), with donor written informed consent ob-

566   tained according to the Declaration of Helsinki. Healthy donor blood samples were obtained from the blood

567   bank at Rigshospitalet, Copenhagen, Denmark. All samples were obtained anonymously

Author Contributions

569   NPK, CH, and SAT performed experiments, analyzed data, generated figures, and wrote the manuscript.

570   AB conducted all bioinformatics analyses and generated figures. AD and MDC performed experiments and

571   analyzed data. IC predicted neoepitopes. KKM conducted structural analyses of pMHC and generated fig-

572   ures. JSH assisted the neopeptide selection and pMHC multimer production. AMB assisted the neopeptide

573   prediction. AKB provided technical guidance. AMM supported data analyses. ZS co-designed in silico

574   platforms and supported funding. NMG assisted in bioinformatic guidance. RA provided patient material,

575   diagnosed and characterized the patients, and generated tumor cell lines. MN designed the in silico plat-

576   forms and supervised neoepitope prediction. GBJ conducted sequencing analysis and discussed data. MD

577   provided patient material, co-supervised the study, and discussed the data. IMS provided patient material,

578   co-supervised the study, discussed the data, and revised the manuscript. SRH conceived the concept, su-

579   pervised the study, discussed the data, and wrote the manuscript.

Data and materials availability

581   All requests for raw and analyzed data and materials will be promptly reviewed by the senior authors to

582   verify whether the request is subject to any intellectual property or confidentiality obligations. Patient-

583   related data not included in the main manuscript or supplementary files may be subject to patient confiden-

584   tiality. Any data and materials that can be shared will be released via material transfer agreement and data

585   processing agreements, provided approval from the relevant authorities.

Code availability

587   MuPeXi used for neoepitope prediction is available for all users at http://www.cbs.dtu.dk/services/MuPeXI/

588   and published in (20). Visualization of pMHCs were generated as described in methods. Analysis of DNA-

barcodes was performed as described in methods, and the bioinformatics pipeline is available at https://ser-vices.healthtech.dtu.dk/service.php?Barracoda-1.8. Code used for further analysis and visualization was written in R as performed as described in methods.

Acknowledgments

References

1. Rosenberg SA, et al. Durable complete responses in heavily pretreated patients with metastatic melanoma using T-cell transfer immunotherapy. *Clin. Cancer Res.* 2011;17(13):4550–4557.

2. Besser MJ, et al. Adoptive transfer of tumor-infiltrating lymphocytes in patients with metastatic melanoma: Intent-to-treat analysis and efficacy after failure to prior immunotherapies. *Clin. Cancer Res.* 2013;19(17):4792–4800.

3. Itzhaki O, et al. Establishment and large-scale expansion of minimally cultured young tumor infiltrating lymphocytes for adoptive transfer therapy. *J. Immunother.* 2011;34(2):212–220.

4. Andersen R, et al. Long-lasting complete responses in patients with metastatic melanoma after adoptive cell therapy with tumor-infiltrating lymphocytes and an attenuated IL-2 regimen. *Clin. Cancer Res.* 2016;22(15):3734–3745.

5. Lauss M, et al. Mutational and putative neoantigen load predict clinical benefit of adoptive T cell therapy in melanoma. *Nat. Commun.* 2017;8(1):1–10.

611 6. Goodman AM, et al. Tumor mutational burden as an independent predictor of response to
612 immunotherapy in diverse cancers. *Mol. Cancer Ther.* 2017;16(11):2598–2608.

613 7. Samstein RM, et al. Tumor mutational load predicts survival after immunotherapy across multiple cancer
614 types. *Nat. Genet.* 2019;51(2):202–206.

615 8. Donia M, et al. Methods to Improve Adoptive T-Cell Therapy for Melanoma: IFN-γ Enhances Anticancer
616 Responses of Cell Products for Infusion. *J. Invest. Dermatol.* 2013;133(2):545–552.

617 9. Rosenberg SA, et al. Treatment of patients with metastatic melanoma with autologous tumor-infiltrating
618 lymphocytes and interleukin 2. *J. Natl. Cancer Inst.* 1994;86(15):1159–1166.

619 10. Zhou J, et al. Persistence of multiple tumor-specific T-cell clones is associated with complete tumor
620 regression in a melanoma patient receiving adoptive cell transfer therapy. *J. Immunother.* 2005;28(1):53–
621 62.

622 11. Lu YC, et al. Mutated PPP1R3B is recognized by T cells used to treat a melanoma patient who
623 experienced a durable complete tumor regression. *J Immunol* 2013;190(12):6034–6042.

624 12. Lu YC, et al. Efficient identification of mutated cancer antigens recognized by T cells associated with
625 durable tumor regressions. *Clin. Cancer Res.* 2014;20(13):3401–3410.

626 13. Huang J, et al. T Cells Associated with Tumor Regression Recognize Frameshifted Products of the
627 CDKN2A Tumor Suppressor Gene Locus and a Mutated HLA Class I Gene Product . *J. Immunol.*
628 2004;172(10):6057–6064.

629 14. Robbins PF, et al. Mining exomic sequencing data to identify mutated antigens recognized by
630 adoptively transferred tumor-reactive T cells. *Nat. Med.* 2013;19(6):747–752.

631 15. Prickett TD, et al. Durable complete response from metastatic melanoma after transfer of autologous T
632 cells recognizing 10 mutated tumor antigens. *Cancer Immunol. Res.* 2016;4(8):669–678.

633   16. Newell EW, et al. Combinatorial tetramer staining and mass cytometry analysis facilitate T-cell epitope

634   mapping and characterization. *Nat. Biotechnol.* 2013;31(7):623–629.

635   17. Joglekar AV, et al. T cell antigen discovery via signaling and antigen-presenting bifunctional receptors.

636   *Nat. Methods* 2019;16(2):191–198.

637   18. Kula T, et al. T-Scan: A Genome-wide Method for the Systematic Discovery of T Cell Epitopes. *Cell*

638   2019;178(4):1016-1028.e13.

639   19. Bentzen AK, et al. Large-scale detection of antigen-specific T cells using peptide-MHC-I multimers

640   labeled with DNA barcodes. *Nat. Biotechnol.* 2016;34(10):1037–1045.

641   20. Bjerregaard AM, et al. MuPeXI: prediction of neo-epitopes from tumor sequencing data. *Cancer*

642   *Immunol. Immunother.* 2017;66(9):1123–1130.

643   21. Wells DK, et al. Key Parameters of Tumor Epitope Immunogenicity Revealed Through a Consortium

644   Approach Improve Neoantigen Prediction. *Cell* 2020;183(3):818-834.e13.

645   22. Jurtz V, et al. NetMHCpan-4.0: Improved Peptide–MHC Class I Interaction Predictions Integrating

646   Eluted Ligand and Peptide Binding Affinity Data. *J. Immunol.* 2017;199(9):3360–3368.

647   23. Rodenko B, et al. Generation of peptide-MHC class I complexes through UV-mediated ligand

648   exchange. *Nat. Protoc.* 2006;1(3):1120–1132.

649   24. Toebes M, et al. Design and use of conditional MHC class I ligands. *Nat. Med.* 2006;12(2):246–251.

650   25. Kvistborg P, et al. TIL therapy broadens the tumor-reactive CD8+ T cell compartment in melanoma

651   patients. *Oncoimmunology* 2012;1(4):409–418.

652   26. Ellebaek E, et al. Adoptive cell therapy with autologous tumor infiltrating lymphocytes and low-dose

653   Interleukin-2 in metastatic melanoma patients. *J. Transl. Med.* 2012;10(1):1–12.

654   27. Effern M, et al. Adoptive T Cell Therapy Targeting Different Gene Products Reveals Diverse and

655 Context-Dependent Immune Evasion in Melanoma. *Immunity* 2020;53(3):564-580.e9.

656 28. Robbins PF, et al. Cutting Edge: Persistence of Transferred Lymphocyte Clonotypes Correlates with

657 Cancer Regression in Patients Receiving Cell Transfer Therapy. *J. Immunol.* 2004;173(12):7125–7130.

658 29. Frahm N, et al. Extensive HLA class I allele promiscuity among viral CTL epitopes. *Eur. J. Immunol.*

659 2007;37(9):2419–2433.

660 30. Gros A, et al. Prospective identification of neoantigen-specific lymphocytes in the peripheral blood of

661 melanoma patients. *Nat. Med.* 2016;22(4):433–438.

662 31. Mcgranahan N, et al. Clonal neoantigens elicit T cell immunoreactivity and sensitivity to immune

663 checkpoint blockade. *Science* 2016;351(6280):1463–1469.

664 32. Hodis E, et al. A landscape of driver mutations in melanoma. *Cell* 2012;150(2):251–263.

665 33. Parkhurst MR, et al. Unique neoantigens arise from somatic mutations in patients with gastrointestinal

666 cancers. *Cancer Discov.* 2019;9(8):1022–1035.

667 34. Bjerregaard AM, et al. An analysis of natural T cell responses to predicted tumor neoepitopes. *Front.*

668 *Immunol.* 2017;8(NOV):1–9.

669 35. Yu G, et al. ClusterProfiler: An R package for comparing biological themes among gene clusters. *Omi.*

670 *A J. Integr. Biol.* 2012;16(5):284–287.

671 36. Cabrita R, et al. Tertiary lymphoid structures improve immunotherapy and survival in melanoma.

672 *Nature* 2020;577(7791):561–565.

673 37. Liu S, et al. Efficient identification of neoantigen-specific T-cell responses in advanced human ovarian

674 cancer. *J. Immunother. Cancer* 2019;7(1):1–17.

675 38. Crowther MD, et al. Genome-wide CRISPR–Cas9 screening reveals ubiquitous T cell cancer targeting

676 via the monomorphic MHC class I-related protein MR1. *Nat. Immunol.* 2020;21(2):178–185.

677 39. Krishna S, et al. Stem-like CD8 T cells mediate response of adoptive cell immunotherapy against human

678 cancer. *Science* 2020;370(6522):1328–1334.

679 40. Carreno BM, et al. A dendritic cell vaccine increases the breadth and diversity of melanoma neoantigen-

680 specific. *Science* 2015;348(6236):803–808.

681 41. Lövgren T, et al. Complete and long-lasting clinical responses in immune checkpoint inhibitor-resistant,

682 metastasized melanoma treated with adoptive T cell transfer combined with DC vaccination.

683 *Oncoimmunology* 2020;9(1).

684 42. Jansen CS, et al. An intra-tumoral niche maintains and differentiates stem-like CD8 T cells. *Nature*

685 2019;576(7787):465–470.

686 43. Borst J, et al. CD4+ T cell help in cancer immunology and immunotherapy. *Nat. Rev. Immunol.*

687 2018;18(10):635–647.

688 44. Dudley ME, et al. CD8+ enriched "Young" tumor infiltrating lymphocytes can mediate regression of

689 metastatic melanoma. *Clin. Cancer Res.* 2010;16(24):6122–6131.

690 45. Hadrup SR, Newell EW. Determining T-cell specificity to understand and treat disease. *Nat. Biomed.*

691 *Eng.* 2017;1(10):784–795.

692 46. Sarkizova S, et al. A large peptidome dataset improves HLA class I epitope prediction across most of

693 the human population. *Nat. Biotechnol.* 2020;38(2):199–209.

694 47. Donia M, et al. Simplified protocol for clinical-grade tumor-infiltrating lymphocyte manufacturing with

695 use of the Wave bioreactor. *Cytotherapy* 2014;16(8):1117–1120.

696 48. Saini SK, et al. Empty peptide-receptive MHC class I molecules for efficient detection of antigen-

697 specific T cells. *Sci. Immunol.* 2019;4(37).

698 49. Krueger F. Trim Galore. *GitHub Repos.* 2012;

699   50. Li H, Durbin R. Fast and accurate short read alignment with Burrows-Wheeler transform.
700   *Bioinformatics* 2009;25(14):1754–1760.

701   51. Broad Institute. Picard Toolkit. *GitHub Repos.* 2019;

702   52. Bray NL, et al. Near-optimal probabilistic RNA-seq quantification. *Nat. Biotechnol.* 2016;34(5):525–
703   527.

704   53. Szolek A, et al. OptiType: Precision HLA typing from next-generation sequencing data. *Bioinformatics*
705   2014;30(23):3310–3316.

706   54. Favero F, et al. Sequenza: Allele-specific copy number and mutation profiles from tumor sequencing
707   data. *Ann. Oncol.* 2015;26(1):64–70.

708   55. Wang S. Copynumber. *GitHub Repos.* 2020;

709   56. Roth A, et al. PyClone: Statistical inference of clonal population structure in cancer. *Nat. Methods*
710   2014;11(4):396–398.

711   57. Xu Q, et al. Design of 240,000 orthogonal 25mer DNA barcode probes. *Proc. Natl. Acad. Sci.*
712   2009;106(7):2289–2294.

713   58. Kivioja T, et al. Counting absolute numbers of molecules using unique molecular identifiers. *Nat.*
714   *Methods* 2012;9(1):72–74.

715   59. Jensen KK, et al. TCRpMHCmodels: Structural modelling of TCR-pMHC class I complexes. *Sci. Rep.*
716   2019;9(1):1–12.

717   60. Lefranc MP, et al. IMGT®, the international ImMunoGeneTics information system R 25 years on.
718   *Nucleic Acids Res.* 2015;43(D1):D413–D422.

719   61. Liebschner D, et al. Macromolecular structure determination using X-rays, neutrons and electrons:
720   Recent developments in Phenix. *Acta Crystallogr. Sect. D Struct. Biol.* 2019;75:861–877.

721 62. Li L, et al. DelPhi: a comprehensive suite for DelPhi software and associated resources. *BMC Biophys.*

722 2012;5(1):9.

723 63. Love MI, et al. Moderated estimation of fold change and dispersion for RNA-seq data with DESeq2.

724 *Genome Biol.* 2014;15(12):1–21.

725 64. Yu G, Hu E. enrichplot: Visualization of Functional Enrichment Result [Internet]2020;https://yulab-

726 smu.top/biomedical-knowledge-mining-book/. cited

727 65. Donia M, et al. Aberrant expression of MHC class II in melanoma attracts inflammatory tumor-specific

728 CD4+T-cells, which dampen CD8+T-cell antitumor reactivity. *Cancer Res.* 2015;75(18):3747–3759.

729

730

731

732

733

734

735

736

737

738

739

740

741
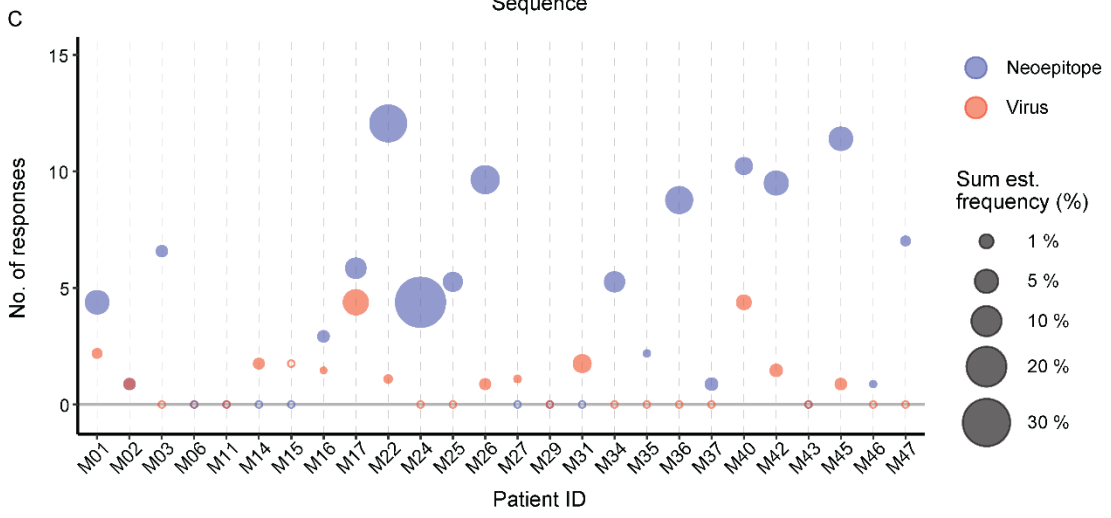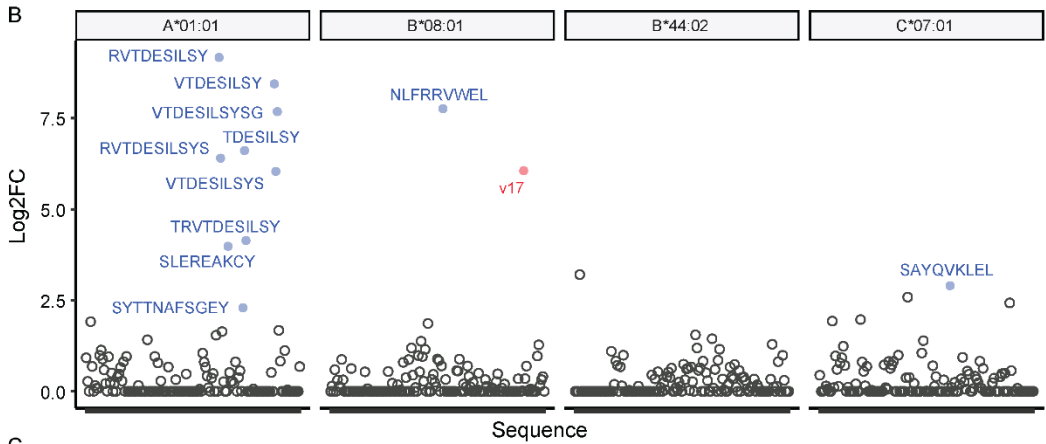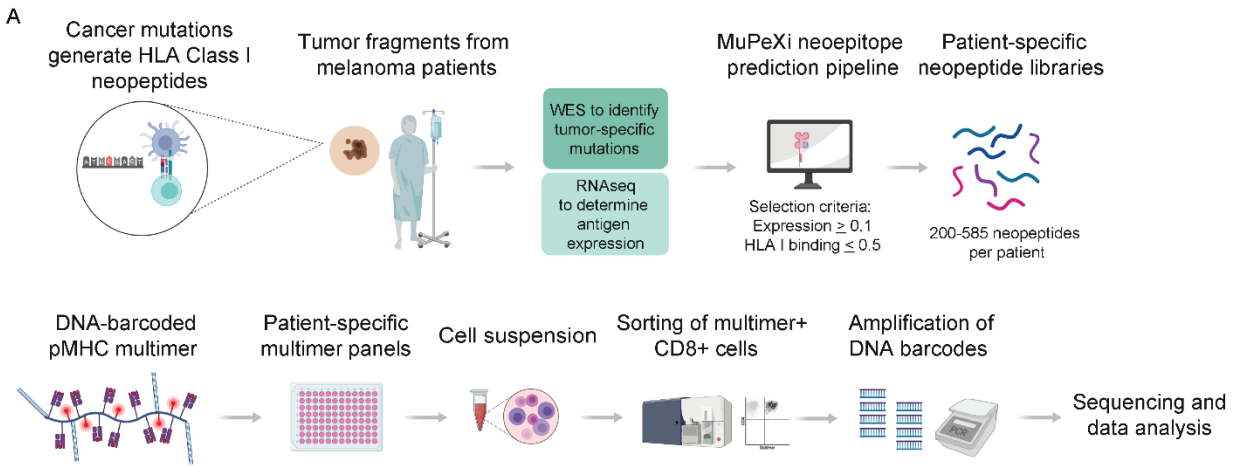
Figures

Figure 1. Detection of neoepitope-specific CD8+ T cells in expanded tumor-infiltrating lymphocytes of melanoma. (**A**) Melanoma-specific mutation-derived peptides were predicted to bind patient's HLA molecules using the prediction platform MuPeXI. DNA barcode-labelled MHC-multimers with either neopeptides or virus-derived peptides were assembled on a PE-labelled streptavidin-conjugated dextran backbone. Multimer-binding, neoepitope-specific CD8+ T cells (NARTs) were fluorescence-sorted and T cell specificities decoded by barcode sequencing. (**B**) Example of neoepitope- and virus-specific CD8+ T cells detected in expanded TILs of melanoma patient M22, partial responder, across available HLAs. Significant barcode enrichment is defined based on a log fold change (log2FC) of the number of barcode reads compared with triplicate baseline samples, and $p \leq 0.001$ (egdeR) after correction for multiple hypothesis testing (see methods). Blue: NARTs; Red: Virus-specific CD8+ T cells; Black: Multimers with non-enriched barcodes. V17 annotate EBV peptide RAKFKQLL. (**C**) Number and frequency of neoepitope- and virus-specific CD8+ T cells in TIL samples across cohort of 26 melanoma patients. Blue: NARTs. Red: Virus-specific CD8+ T cells. Number of and frequency of NARTs were normalized to absolute HLA coverage (see methods).

768
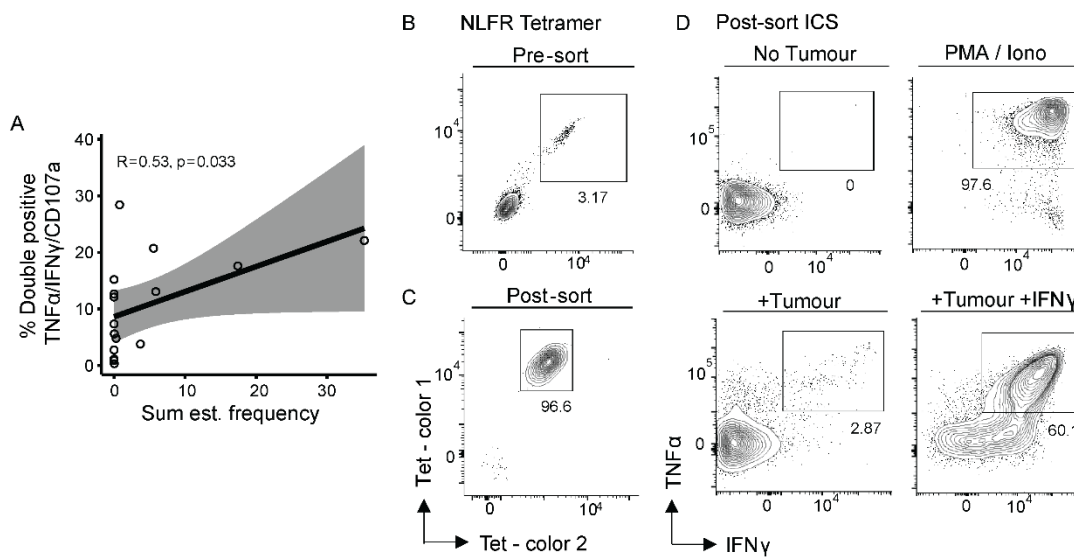
Figure 2. Autologous tumor recognition by enriched NARTs. (**A**) Correlation of TIL reactivity to autologous tumor (measured by ICS) and sum of estimated NART frequency. TIL reactivity towards an autologous tumor cell line was defined as positive for two out of TNFα, IFNγ and CD107a. 16 patients with available tumor reactivity data were included from both responder (n = 6) and non-responders (n = 10). R and p-value from Spearman correlation with 95% confidence intervals in grey. NART frequency was normalized to absolute HLA coverage (see methods). (**B-C**) HLA-B*08:01-restricted, NLFR specific CD8+ T cells from M22 TIL Inf product were sorted based on 2-color tetramer binding (**B**) and expanded in vitro followed by NLFR-tetramer staining (**C**). (**D**) Tumor reactivity as measured by TNFα/IFNγ release after co-culture of expanded, NART-specific cell products with, or without autologous tumor cell lines, with PMA/Ionomycin, or with autologous tumor cell line and IFNγ. NLFR, NLFRRVWEL from USP34[S1391F]. ICS, intracellular cytokine staining. TIL reactivity data shown in A originate from (4) and the assay performed as described in (65).

782

783

784

785
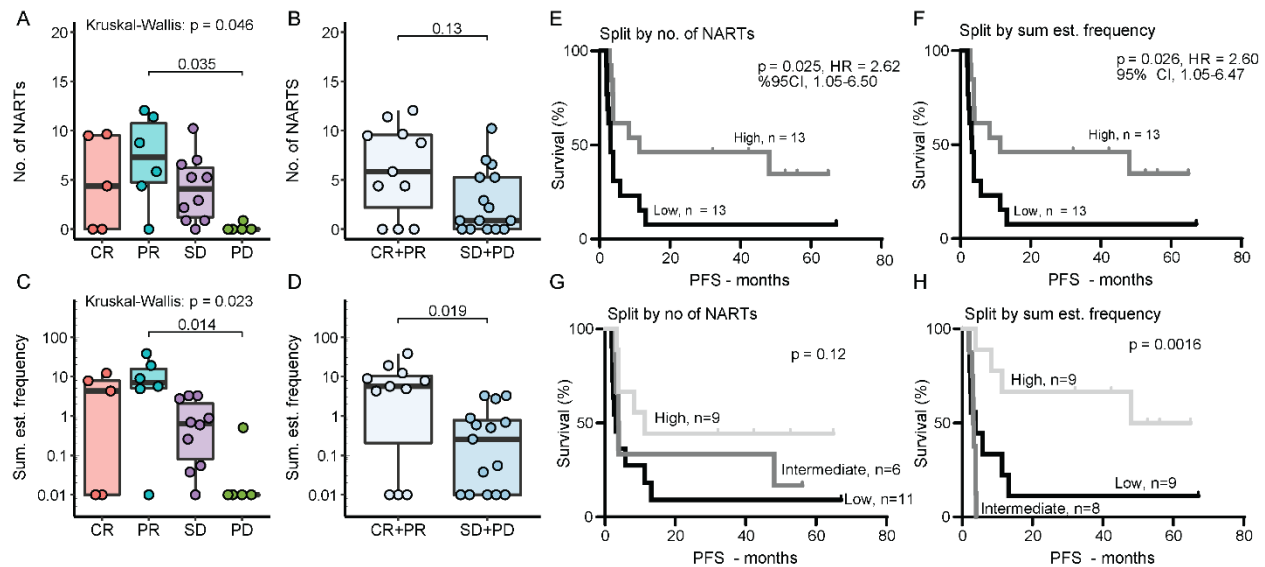
Figure 3. Frequency of NARTs correlate with increased survival after TIL-ACT. (**A-B**) NART diversity represented as the number of NARTs detected in TIL Inf products for each patient according to RECIST (**A**) and clinical response (**B**). (**C-D**) NART frequency represented as the sum of estimated frequency of NARTs detected in TIL Inf products for each patient according to RECIST (**C**) and clinical response (**D**). (**E-F**) Progression-free survival for the cohort split by the median NART diversity (median = 3.65 NARTs) (**E**) and median NART frequency (median = 0.63 %) (**F**). (**G-H**) Progression-free survival for the cohort splits by high (> 66th percentile), intermediate (> 33rd percentile), and low groups (≤ 33rd percentile). (**G**), NART diversity. 66th percentile = 5.65 NARTs. 33rd percentile = 0.88 NARTs. (**H**), NART frequency. 66th percentile = 3.26%. 33rd percentile = 0.03%. p-values were calculated using Kruskal-Wallis test followed by Dunn's multiple comparison test in A and C; only significant comparisons are shown. Non-parametric Mann-Whitney U test was used for B and D. Boxplot whiskers represent IQR. p-values and hazard ratios (HR) were calculated using Mantel-Cox test and log-rank approach, respectively in E-H. Both number of and frequency of NARTs were normalized to absolute HLA coverage (see methods). n = 26 for all plots. All values displayed on a logarithmic scales were increased by 0.01 to account for zero-values
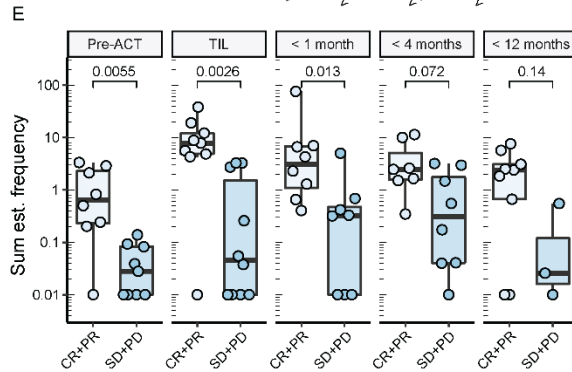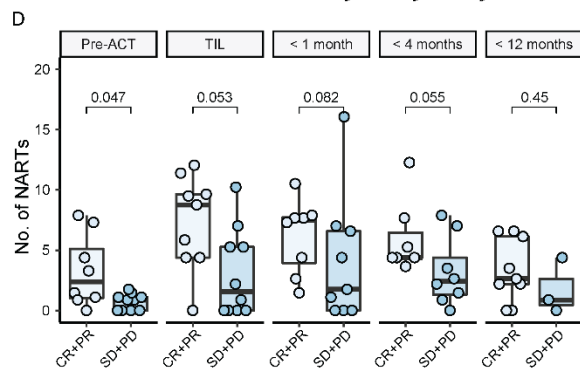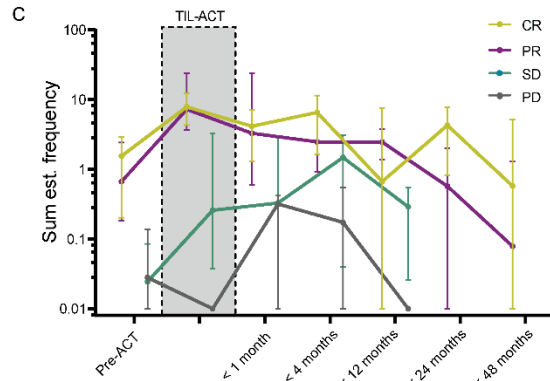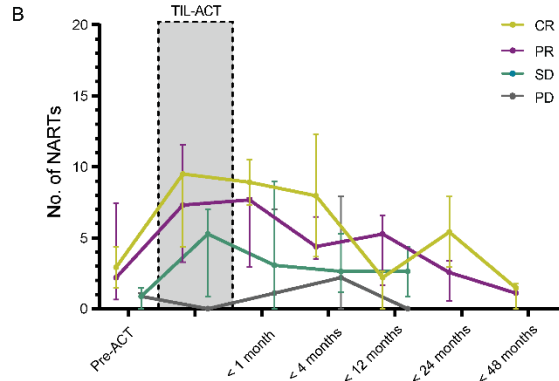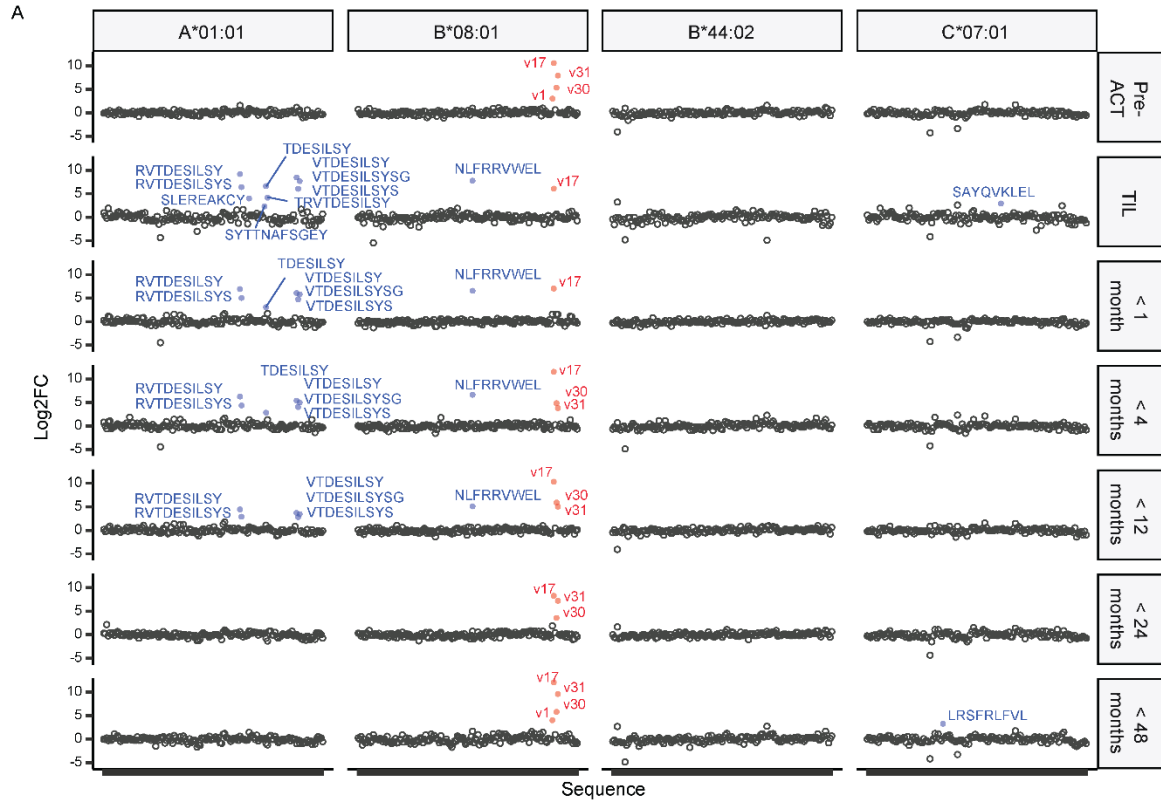
Figure 4. NARTs appear in peripheral blood and decline in frequency following TIL-ACT.
(**A**) Output example from screening paired PBMCs from 19 patients. Virus- and neoepitope-specific CD8+ T cells in patient M22 (PR) in Pre-ACT PBMCs, TIL Inf product, and PBMCs following TIL-ACT. Blue: NARTs. Red: Virus-specific CD8 T cells. Black: Multimers associated with non-enriched barcodes. Significant barcode enrichment is defined based on a log2FC of the number of barcode reads compared with triplicate baseline samples, and p < 0.001 (egdeR) (see methods). V1 annotate FLU peptide ELRSRYWAI, v17 annotate EBVvirus peptide RAKFKQLL, v30 annotate EBV peptide QAKWRLQTL, and v31 annotated EBV peptide FLRGRAYGL. (**B-C**) Median number of NARTs, error bars indicate IQR, points were displaced for visual purposes. **(B)** and sum of estimated NART frequency **(C)** over time in TIL Inf product and available PBMC samples. Patients are divided according to RECIST groups. (**D-E**) Boxplots representing diversity **(D)** and frequency **(E)** of NARTs for each patient according to RECIST groups. p-values were calculated using Mann-Whitney U test. 19 patients had both TIL Inf products and PBMCs available, but the number of samples at each time point varied according to sample and data availability (Supplemental Table 1, Supplemental Figure 8). NART frequency could not be calculated for M40 PBMCs Pre-ACT and for M40 PBMCs < 1 month after treatment (see methods) and are therefore excluded in C and E. Whiskers represent IQR. NART frequencies were normalized to HLA coverage of the given patient (see methods). All values displayed on logarithmic scales were increased by 0.01 to account for zero-values.
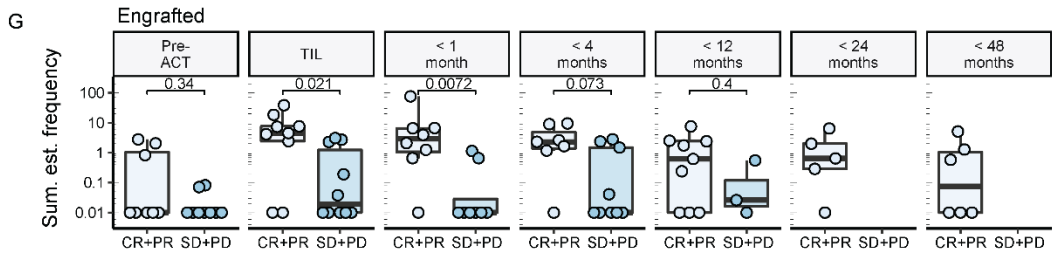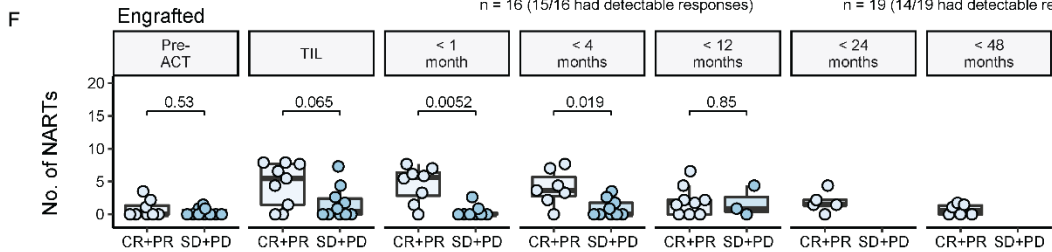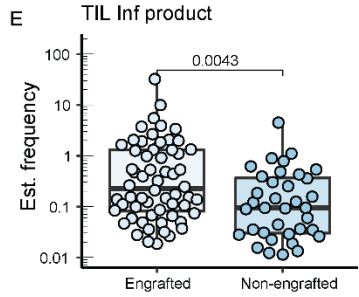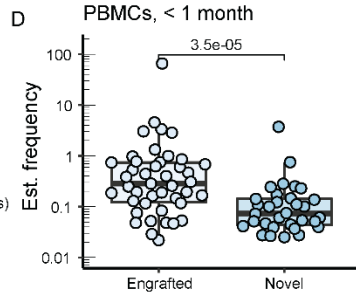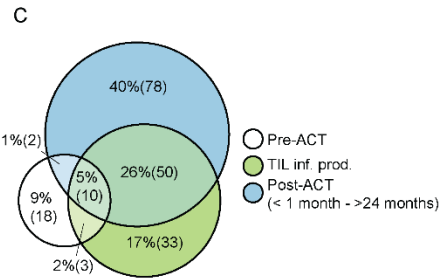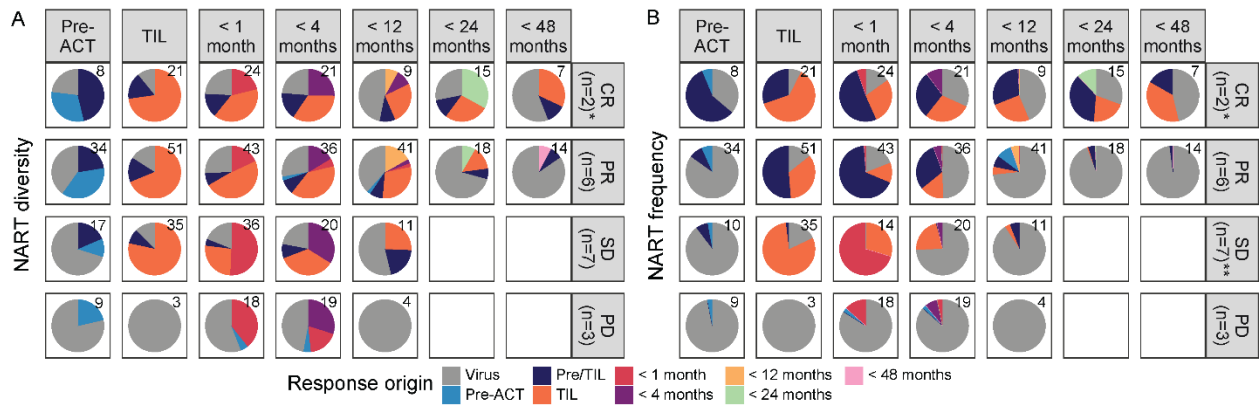
832

833

834

835

836

837

40

Figure 5. Responding patients have high frequent, engrafting NARTs in their TIL infusion product. (**A-B**) Each NART population was annotated and colored according to first appearance in Pre-ACT PBMCs, TIL Inf products and Post-ACT PBMCs (< 1 month to < 48 months). Black numbers specify the total number of NARTs detected at the specific time and RECIST group. (**A**) Distribution of NARTs within RECIST groups according to first appearance. (**B**) Distribution of NART frequency within RECIST groups according to first appearance. *M01 (CR) did not have pre-ACT and < 1 month PBMCs available and was excluded from analysis to avoid a biased distribution. **Frequency data could not be calculated for M40 pre-ACT, and M40 post-ACT < 1 month, which were excluded (see methods). (**C**) Venn diagram showing the overlap of detected NARTs between pre-ACT PBMCs, TIL Inf products and all post-ACT PBMC samples. n = 19. (**D**) The estimated frequency of each NART population detected < 1 month post infusion. Responses were either regarded as engrafted (i.e. also detected in TIL Inf) or novel. n = 16, M01 and M40 were excluded as stated for (A-B), M29 did not have detectable antigen-specific CD8 T cells before the second time point post-ACT (**E**) The estimated frequency of each NART population observed in TIL Inf products. Non-engrafted vs engrafted (i.e. detected at least once at a later time points), n=19. (**F-G**) Number and frequency of engrafted NARTs, defined by presence in both TIL Inf product and post TIL-ACT. n varied according to sample availability (Supplemental Table 1, Supplemental Figure 8). M40 pre-ACT and < 1 month PBMCs were excluded from G (see methods). Sum of estimated frequency in G was increased by 0.01 to account for zero-values. p-values from Mann-Whitney U test. Whiskers represent IQR.

863
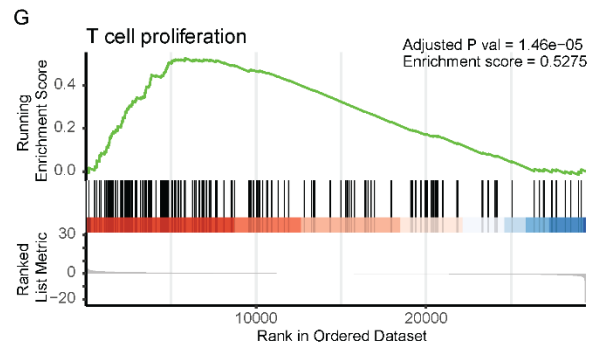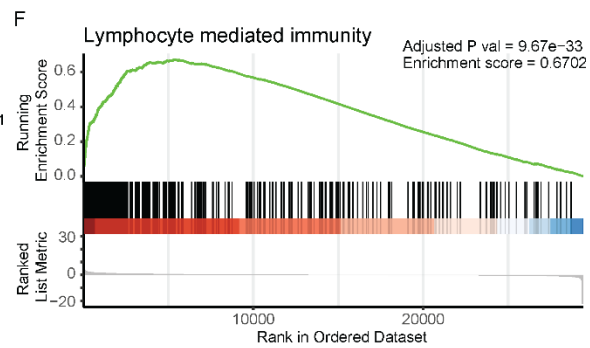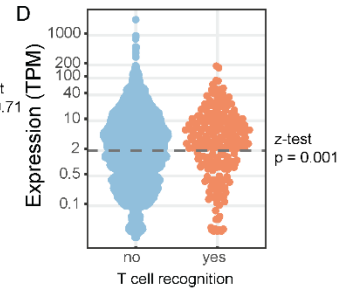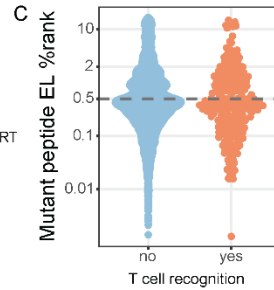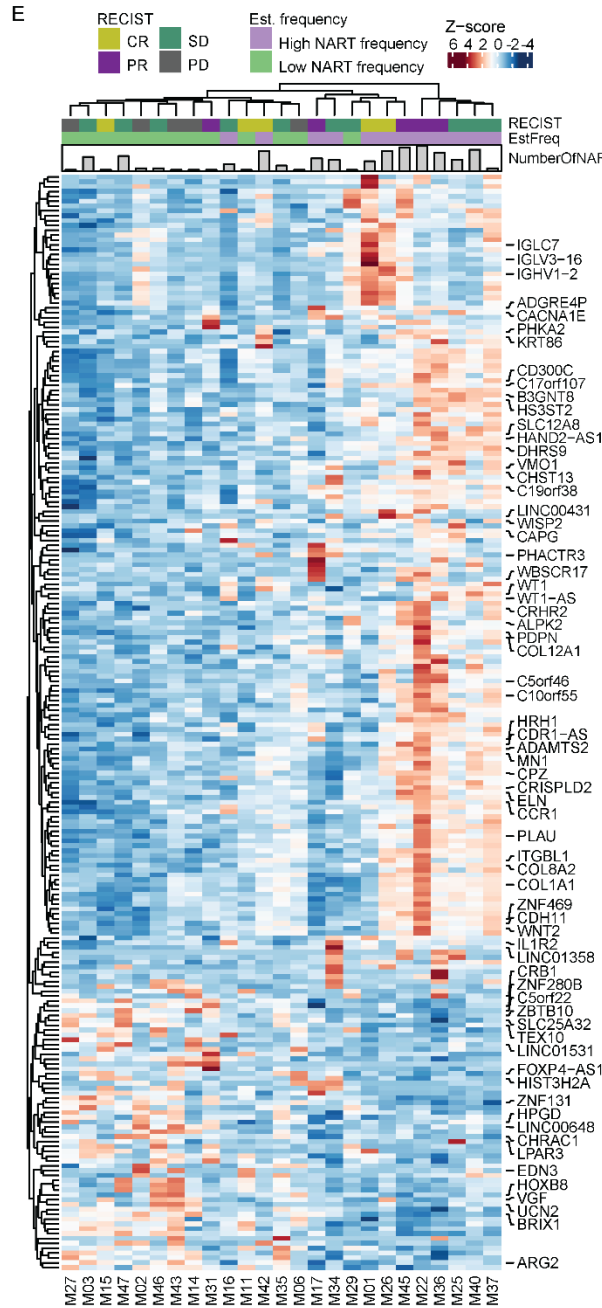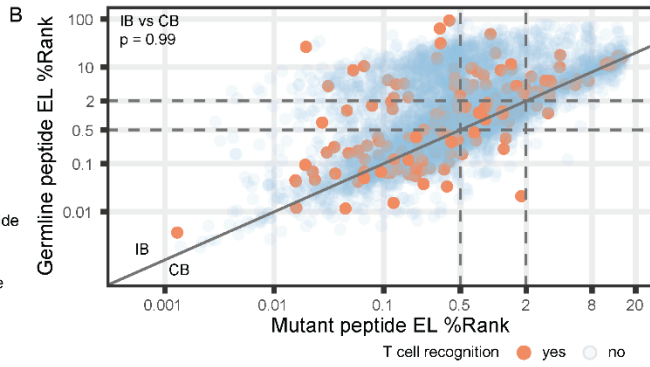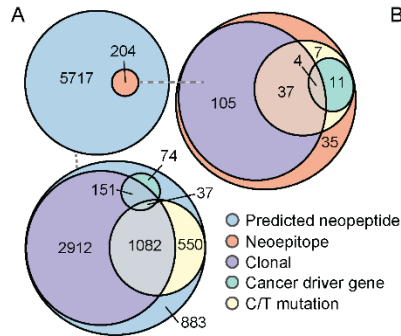
Figure 6. Characteristics of immunogenic neoepitopes. (**A**) Venn diagram of 5921 unique pMHC; 204 immunogenic and 5717 non-immunogenic as determined by the presence of neoepitope-specific CD8+ T cells in patients at any time. The distribution and overlap of immunogenic vs. non-immunogenic neoepitopes deriving from either cancer driver genes (6.5% vs. 3.3%, p = 0.0048, z-test), C/T mutations (3.4% vs. 3.5%, p = 0.78, z-test), and clonal mutations (80.1% vs 86.0%p =0.03, z-test). Clonality could not be determined for 913 neopeptides as WES was performed on autologous tumor cell lines (M22, M24, and a subset of M15). These were excluded from the *z*-test, but included in the Venn diagram as subclonal mutations for visualization. (**B**) Eluted ligand (EL) %rank of mutated peptide compared to %rank of the corresponding germline peptide without mutation or nearest germline peptide, immunogenic peptides are colored red (3.4% CB vs. 3.5 % IB, *p*-value = 0.99, *z*-test). (**C**) Mutant EL %rank comparing proportion of immunogenic neoepitopes above and below 0.5 %rank (3.3 % vs 3.5, *p*-value = 0.71, *z*-test). (**D**) RNA expression (TPM), comparing proportion of immunogenic peptides with expression above and below 2 TPM (4.2 % vs. 2.6%, *p*-value = 0.001, *z*-test). (**E**) Unsupervised clustering of the 226 differential expressed gene according to high and low sum of estimated frequency within TIL Inf products split by the median frequency (0.63%). Denoted names were prioritized according to GO terms and known function. (**F**) Enriched GO gene set representing lymphocyte-mediated immunity. (**G**) Enriched GO gene set representing T cell proliferation. Significance thresholds for GSEA was set at FDR ≤ 0.01. M24 was excluded from D-G as RNAseq data was obtained from an autologous tumor cell line, n = 25. M22 was included in D-G using data from the tumor biopsy used for manufacturing of the infusion product.